FEM Simulation and Experimental Testing of a CHUD Combiner Unit Geometry

Ricardo Puerta da Costa Lima Guedes

Dissertação de Mestrado

Orientador na FEUP: Prof. José Manuel Ferreira Duarte

Orientador na empresa: Eng. Rui Barros

FEUP FACULDADE DE ENGENHARIA
UNIVERSIDADE DO PORTO

Mestrado Integrado em Engenharia Mecânica

Julho de 2019

“You must always strive to be the best, but you must never believe that you are.”

Juan Manuel Fangio

Resumo

Nos últimos anos tem-se verificado um aumento crescente dos sistemas *infotainment* nos veículos automóveis. Este trabalho desenvolveu-se no âmbito de um destes sistemas, de nome *Combiner Head-up Display,* mais especificamente na análise do sub-sistema *combiner unit* produzido pela BOSCH Car Multimédia Portugal, S.A. Este produto é desenvolvido para o novo FORD Focus, que teve início de comercialização em 2018.

O *combiner unit* é composto por 3 componentes: *combiner*, *combiner support* e o adesivo. O *combiner* é produzido num material opticamente transparente, policarbonato, e é responsável pela criação da imagem virtual para o condutor. O *combiner support* é fabricado por injeção e é um compósito de matriz de poliamida reforçada com fibra de vidro e, tem como papel fixar o *combiner* no sistema CHUD. O adesivo é uma resina epoxy e constitui o elemento de ligação entre os dois outros componentes.

O modo de funcionamento deste conjunto depende fortemente da capacidade de criação de uma imagem virtual de qualidade no *combiner*. A qualidade da imagem depende da geometria final do *combiner unit*. Neste momento, vários fatores têm condicionado a qualidade (geometria final) deste produto. Destes são de salientar: *Combiner* e *combiner support* fornecidos fora de especificação e alteração de geometria durante o processo de fabrico.

Tendo o problema identificado, o objetivo deste trabalho foi analisar o desvio da superfície do *combiner* tendo em conta a influência do processo de colagem, da camada de adesivo e, por fim, o desvio do *combiner support* quando comparado com as medidas nominais.

Na fase inicial deste trabalho foi realizado o levantamento geométrico de todos os componentes a utilizar. Para tal, uma máquina de medição de coordenadas, também conhecida por CMM, foi utilizada para compreender os desvios existentes no *combiner support*, enquanto que para o *combiner*, a análise foi realizada usando um scanner 3D, ou seja de levantamento de forma, permitindo assim o rastreamento do desvio da superfície da peça comparativamente às medidas nominais, antes e depois do processo de colagem. Verificou-se que a grande maioria se encontrava fora de especificação.

Com o objetivo de prever a geometria final do *combiner* após colagem foi desenvolvido um modelo de simulação baseado no Método de Elementos Finitos, usando como ferramenta o ABAQUS CAE. Neste modelo a análise é feita a partir de uma casca da superfície do *combiner* e a variação dos pontos de contacto entre o *combiner* e o *combiner support*. Desta maneira, é possível criar uma previsão da deformação dos *combiners* baseado nas especificações do *combiner support*. Para validação do modelo numérico foram utilizadas duas metodologias: na primeira uma série de *combiner supports* foram modificados e na segunda o desenvolvimento de um JIG no qual as condições impostas no modelo de simulação do ABAQUS CAE fossem replicadas. Estes estudos permitiram uma validação qualitativa dos resultados obtidos numericamente. Esta validação consistiu na comparação dos dois resultados experimentais com os resultados numéricos. Até ao momento não foi possível introduzir a influência do adesivo no modelo numérico. Para aumentar a realidade dos resultados da simulação será necessário em trabalhos futuros considerar este parâmetro.

FEM Simulation and Experimental Testing of a CHUD Combiner Unit Geometry

Abstract

In the last years there has been an incresing growth of the infotainment systems in the automotive vehicles. This thesis was developed in the context of one of these systems, named Combiner Head-up Display, more specifically in the analysis of the sub-system combiner unit produced by BOSCH Car Multimedia Portugal, S.A. This product is developed for the new FORD Focus which began its commercialization in 2018.

The combiner unit is composed by three components: combiner, combiner support and the adhesive. The combiner is produced in an optically transparent material, polycarbonate, responsible for the creation of the virtual image for the driver. The combiner support is fabricated by injection and it's a fiber glass reinforced polyamide matrix composite, which is responsible for fixing the combiner in the CHUD system. The adhesive is an epoxy resin and constitutes the bonding element between the other two components.

The working principle of this assembly strongly depends on the capacity of a quality virtual image creation in the combiner. The image quality depends on the fina geometry of the combiner unit. At the moment, several factors have been conditioning the quality (final geometry) of this product. Of these it's to be noted: the combiner and combiner support being supplied out of specification and the geometry alteration during the fabrication process.

Having identified the problem, the objective of this work was to analyse the combiner surface deviation taking into account the influence of the gluing process, the adhesive layer and, lastly, the deviation of the combiner support when compared with the nominal measures.

In the initial phase of this work the geometric mapping of all the components to be used was done. To do such, a coordinates measuring machine, also known as CMM, was used to understand the existing deviations in the combiner support, while for the combiner, the analysis was realized using a 3D scanner, in other words surface shape mapping, allowing the tracking of the part surface deviation comparatively to the nominal surfaces, before and after the gluing process. It was verified that most of the parts were out of specification.

With the objective of forecasting the final geometry of the combiner after gluing, a simulation model based on the Finite Elements Method was developed, using the ABAQUS CAE software. In this model, the analysis is done considering a shell of the combiner surface and the variation of the contact points between the combiner and combiner support. This way, it's possible to create a forecast of the combiners deformation based on the combiner supports specifications. For the validation of the numerical model were utilized two methodologies: in the first a series of combiner supports were modified and, in the second a JIG was developed in which the imposed conditions in the ABAQUS CAE simulation model were replicated. These studies allowed the qualitative validation of the results obtained numerically. Till now, it was not possible to introduce the adhesive influence in the numerical model. To increase the reality of the simulation results it will be necessary to consider this parameter in the future works.

Acknowledgements

I would like to thank all the people involved in the realization of this master thesis:

To my university mentor at FEUP, Prof. José Ferreira Duarte, for all the help, guidance and fruitful debates we had throughout this work and that made it possible. To all the teachers that helped me during my academic life. Also a special thanks to Armanda from INEGI for using her time helping me with some experimental tests for this project.

To my mentor at BOSCH Car Multimedia, Eng. Rui Barros, who since day one was very supportive and helpful in the realization of this master thesis. Also, to the ECM3 team members Manuel Sarmento, Carlos Oliveira, Filipe Valente, Hernani Abreu, Vasco Pinto, Marcelo Domingues, Pedro Moreira, Daniela Santos and Aníbal Portinha.

To all my friends that entered with me at BOSCH Car Multimedia and helped me with the integration process namely, Carlos Pires, Catarina Almeida, Vânia Silva, Mafalda Varela, Filipe Giesteira, Ana Leça, Gabriel Pinheiro, Pedro, João Martins, Patrícia Gonçalves and Rui Costa.

To my close friends and the ones who gave me all the motivation and support for the success of this project especially to Hipólito, Tinoco, Francisco Taveira Pinto, Gonçalo Hipólito, Sara Loureiro, Teresa Magalhães, Isabel Costa, Vitória Abreu, Diogo Sousa, Abel Santos, Pedro Casas, João Aleluia, Tiago Roque and Inês Beires.

To my team at BBDouro who made me company during the entire time of this master thesis.

To my family that made it possible for me to come so far to this point especially to my parents, my brother and my sister.

And lastly, a special huge thanks to Rui Almeida, who was always backing me up and did all the possible efforts to help me with everything.

Índice de Conteúdos

1 Introduction 1
- 1.1 Project Framework and Motivation 1
- 1.2 Bosch Group 1
- 1.3 Bosch Car Multimedia Portugal, S.A. 2
- 1.4 Project Goals 3
- 1.5 Methodology 4
- 1.6 Structure 5

2 Literature Review 6
- 2.1 A briefing to the car and driver data transmission 6
- 2.2 Head-up Displays (HUD) and how they work 8
- 2.3 Combiner Head-up Display (CHUD) and how they work 9

3 FORD Focus CHUD 12
- 3.1 Combiner 13
- 3.2 Combiner Support 15
- 3.3 Adhesive 17

4 FORD Focus CHUD Combiner and Combiner Support analysis 19
- 4.1 Combiner geometry analysis 19
- 4.2 Combiner Support geometry analysis 23
- 4.3 Combiner Unit assembly process 25
- 4.4 Combiner Unit geometry analysis and typical problem 26
- 4.5 Adhesive thickness testing 29

5 ABAQUS CAE simulation model 35
- 5.1 Introduction to the Finite Element Method 35
- 5.2 Creation of the ABAQUS CAE model simulation 37
- 5.3 Combiners supports modifications and ABAQUS CAE simulation 43

6 Jig development 47
- 6.1 3D printing simulation 48
- 6.2 Jig production 50
- 6.2.1 Base structure 53
- 6.2.2 Top part 55
- 6.3 Working principle of the jig 55

7 Validation of controlled model 57
- 7.1 Height deviation $Delta_z$ (PV Value) results comparison 57
- 7.2 Slopes results comparison 64

8 Conclusions and Future work 70
- 8.1 Final conclusions 70
- 8.2 Future work 71

9 Bibliography 72

Appendix A: Other activities 74

Acronyms

CAE – Complete Abaqus Environment

CHUD – Combiner Heads-Up Display

FDM – Fused Deposit Modeling

FEA – Finite Element Analysis

FEM – Finite Element Method

HUD – Heads-Up Display

INEGI – Institute of Science and Innovation in Mechanical and Industrial Engineering

PLA – Polylatic Acid

PGU – Picture Generation Unit

RPM – Revolutions per Minute

UV – Ultra violet

Figure Index

Figure 1: BOSCH Logo (Bosch, 2019) 1
Figure 2: Highlights of the 2018 business year (Bosch, 2019) 2
Figure 3: BOSCH Car Multimedia Portugal, S.A. 3
Figure 4: BOSCH facts and numbers (Bosch, 2019) 3
Figure 5: Flowchart 5
Figure 6: Ford Model A interior (Mecum, 2019) 6
Figure 7: Peugeot 205 GTi dashboard (Smith, 2019) 7
Figure 8: BMW dashboard (Roze, 2019) 7
Figure 9: HUD in the aviation industry (Evans, 2019) 8
Figure 10: BMW HUD (Nicolazzo, 2019) 9
Figure 11: 2019 FORD Focus CHUD (FORD, 2019) 9
Figure 12: CHUD working principle (Almeida, 2019) 10
Figure 13: BMW Combiner Unit 10
Figure 14: FORD Focus Combiner Unit 11
Figure 15: FORD CHUD Combiner Unit Exploded View (Almeida, 2019) 12
Figure 16: FORD Focus CHUD 13
Figure 17: FORD Focus combiner (McNamara, 2019) 14
Figure 18: FORD CHUD Combiner 14
Figure 19: FORD CHUD Combiner Support 15
Figure 20: Influence of the glass fiber ratio at 20ºC (B. Mouhmida, et al. 2006) 16
Figure 21: Temperature effect on the failure strain with different glass fiber ratios (B. Mouhmida, et al. 2006) 17
Figure 22: One-part epoxy curing process. (ThreeBond, 2019) 18
Figure 23: Two-part epoxy curing process. (ThreeBond, 2019) 18
Figure 24: 3D Shape scanner machine 19
Figure 25: 3D Shape cameras 20
Figure 26: Scheme of the 3D scanner surface analysis 20
Figure 27: Combiner deviation to nominal before the gluing process 21
Figure 28: Working principle of the 3D Shape scanner 21
Figure 29: Combiner 1 before gluing 22
Figure 30: Combiner 8 before gluing 23
Figure 31: Combiner 3 before gluing 23
Figure 32: Combiner 9 before gluing 23
Figure 33: Combiner 2 before gluing 23
Figure 34: Combiner Support 24
Figure 35: P points measuring output 25

Figure 36: Combiner gluing area (blue) and guiding cuts (red). 26
Figure 37: Combiner unit analysis on 3DShape Scanner 27
Figure 38: Combiner 1 after the gluing process. 27
Figure 39: Combiner 8 after the gluing process. 27
Figure 40: Combiner 3 after the gluing process. 28
Figure 41: Combiner 9 after the gluing process. 28
Figure 42: Combiner 2 after the gluing process. 28
Figure 43: Combiner support measured values 29
Figure 44: Band saw machine at FEUP 30
Figure 45: Polishing machine Struers RotoPol-21 at FEUP 30
Figure 46: Combiner samples cut horizontally after the polishing process 31
Figure 47: Combiner samples cut vertically (C2.1 on the left and C2.6 on the right) 31
Figure 48: Olympus PMG3 microscope 32
Figure 49: Chosen measuring points in both types of samples 32
Figure 50: Output data from the Olympus microscope 33
Figure 51: Elements Types (Andujar Moreno , 2019) 35
Figure 52: ABAQUS CAE Example (Ajri, 2019) 36
Figure 53: Brake discs mesh (adapted from Broekaart, 2019) 37
Figure 54: 3D Combiner part in ABAQUS CAE. 38
Figure 55: Combiner 3D middle surface in ABAQUS CAE. 38
Figure 56: Combiner partitions 39
Figure 57: Polycarbonate properties submitted in ABAQUS CAE. 39
Figure 58: Gluing area boundary conditions. 40
Figure 59: Combiner guiding cuts boundary conditions. 40
Figure 60: Displacement in the P points 41
Figure 61: Meshed part 41
Figure 62: Simulation on the full area of the combiner 42
Figure 63: Analysis area of the combiner 42
Figure 64: Approach to the nominal real part 43
Figure 65: ABAQUS simulation of combiner unit 21 45
Figure 66: ABAQUS simulation of combiner unit 22 45
Figure 67: ABAQUS simulation of combiner unit 23 45
Figure 68: ABAQUS simulation of combiner unit 24 46
Figure 69: ABAQUS simulation of combiner unit 25 46
Figure 70: CATIA V5 model of the jig 47
Figure 71: Jig simulation 48
Figure 72: Jig feedrate simulation 49

Figure 73: Selection of the printing parameters 49
Figure 74: Ultimaker S5 3D printer..50
Figure 75: Schematic of a FDM printer (Olivera, 2019)...51
Figure 76: Infill pattern and density (Siber, 2019)...51
Figure 77: Jig components..52
Figure 78: Final product 53
Figure 79: 3D Base model of the jig in CATIA V5 53
Figure 80: Jig base structure holding the combiner..54
Figure 81: Top part of the jig 55
Figure 82: Initial phase of the combiner mounted in the jig 56
Figure 83: Mounted and tightened combiner 56

Table index

Table 1 – Combiner samples peak-to-valley deviation 22
Table 2 – P points nominal measures and respective upper and lower limit 25
Table 3 – Measures from the combiners horizontally 33
Table 4 – Measures from the combiners cut vertically 33
Table 5 – Combiner support modifications 44
Table 6 – Polylatic Acid Properties (Giang, 2019) 48
Table 7 - Combiner Unit 21 measuring results 58
Table 8 - Combiner Unit 22 measuring results 59
Table 9 - Combiner Unit 23 measuring results 60
Table 10 - Combiner Unit 24 measuring results 61
Table 11 - Combiner Unit 25 measured results 62
Table 12 – Diagram of the slope results tables 64
Table 13 - Combiner Unit 21 measured slopes results comparison 65
Table 14 - Combiner Unit 22 measured slopes results comparison 66
Table 15 - Combiner Unit 23 measured slopes results comparison 67
Table 16 - Combiner Unit 24 measured slopes results comparison 68
Table 17 - Combiner Unit 25 measured slopes results comparison 69

1 Introduction

In this first chapter a brief description of Bosch Group and Bosch Car Multimedia, where I had the opportunity to realize the internship, is presented.

Topics like project goals, methodology and thesis structure are also described, as well as the entire framework and motivation for this project.

1.1 Project Framework and Motivation

The internship took place in Braga, at the Bosch Car Multimedia in the mechanical development team CM-CI2/ECM3. The projects of this team rely on the development and support to the production of the FORD and BMW CHUD, which stands for Combiner Head-up Display. The team is also responsible for the CHUD that take part in all MINI models.

Regarding the FORD CHUD, when it comes to the validation of the components the development team is facing some issues concerning ageing tests, like power humidity and thermal cycles. Image distortion was one of the main issues concerning the combiner unit due to the products arriving from the manufacturer out of specification, more precisely the combiner and combiner support, components which will be introduced later on. So the objective was set to create a simulation using Finite Element Methods (FEM) that would allow the team to forecast more efficiently these deformations and lastly, together with the optical department, analyze the results and understand how the image would be deformed.

Knowing I was going to be able to leave my comfort zone for the completion of this project, mainly because I had to study the Finite Element Method and the ABAQUS software, as well as understand some concepts about optical engineering, is what motivated me the most.

1.2 Bosch Group

In 1886, Robert Bosch opened the “Workshop for Precision Mechanics and Electrical Engineering” in Stuttgart, Germany which later would end up to be called Bosch Group.

Figure 1: BOSCH Logo (Bosch, 2019)

Being a global supplier of technology and data, the company employs almost 410000 associates worldwide and is divided into four different business sectors such as:

- Mobility Solutions;
- Industrial Technology;
- Consumer Goods;
- Energy and Building Technology.

Some interesting facts about the company are shown below in Figure 2. Of the 410000 associates 69500 are responsible from the research and development department which is an increase of plus 5200 associates in comparison with 2017. (Bosch R. , 2019)

Figure 2: Highlights of the 2018 business year (Bosch, 2019)

In Portugal, Bosch is present since 1911, being one of the most recognized companies in the country. The three main plants, Bosch Termotecnologia in Aveiro, Bosch Car Multimedia in Braga and Bosch Security Systems in Ovar, develop and produce hot water solutions, automotive multimedia and safety and communication systems, having its headquarters in Lisbon. (Bosch R. , Bosch em Portugal, 2019)

1.3 Bosch Car Multimedia Portugal, S.A.

Having started in 1990, Bosch Car Multimedia in Braga is the leading plant of the Car Multimedia division. Because of the plant great growth, one of the latest achievements was the creation of a development department, as shown in Figure 3. This development center was the main location for the realization of the thesis.

Figure 3: BOSCH Car Multimedia Portugal, S.A.

Bosch is one of the biggest employers in Portugal having 4,800 collaborators and an amount of 1.5 thousand million on sales according to official statistics. Braga plant focus mainly on clusters, Heads-Up displays systems and instruments systems for the two wheeler market.

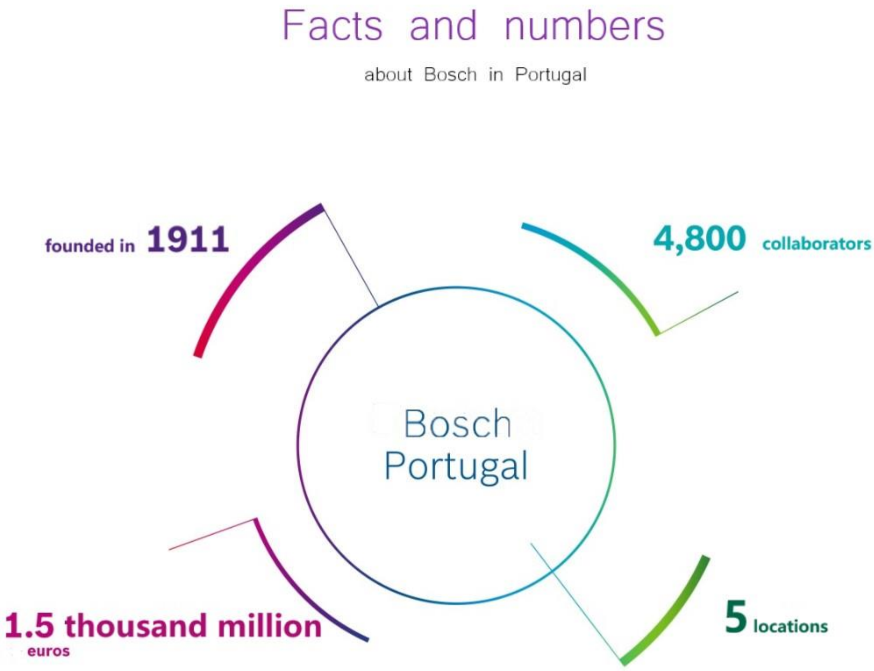

Figure 4: BOSCH facts and numbers (Bosch, 2019)

1.4 Project Goals

This thesis is based on a future work from Rui Almeida's master thesis, Head-up Display Combiner Unit stress and deformation analysis. The main goal is to achieve a Finite Element Analysis (FEA) of the combiner unit geometry resourcing only to the combiner component, taking into account the surface contact points of the combiner support. This can be achieved when the boundary conditions corresponding to the glued combiner are considered. As a result it is expected to observe how the geometry correlates with the size variation of the contact points, also known in this case by control points.

For the realization of this master thesis, the following objectives were set:

- Analyze the geometric stability of the combiner support in different conditions;
- Analyze the shape of the combiner before and after gluing, with normal and modified combiner supports assembled;
- Creation of a simulation model using finite element analysis to achieve a better comprehension of the combiner behavior in a controlled conditions environment;
- Creation of an experimental model to input a displacement in the combiner with known condition;
- Validate the simulation using the experimental model created;
- Arrange a correlation between the combiner geometry and the combiner support shape deviations.

1.5 Methodology

For the successful completion of this master thesis, was fundamental to comprehend the FORD CHUD working principle, as well as the problems associated to it. Despite having two weeks of an integration process at BOSCH in the beginning, the following days were spent in the production line to observe all the process responsible for creating the complete FORD CHUD.

The following task was similar to the first, since a visit to the the optical lab was done in order to gain the know-how of how the optical components are controlled and measured. This involved the comprehension of the working principle of a 3D scanner machine as well as the output data info.

The fourth step was the controlled modification of a number of samples, creating a set of different conditions and so allow the creation of a correlation with the combiner geometry analysis.

The final task was the study of the ABAQUS software and the creation of a simulation model of the combiner unit to analyze its deformation. This was followed by the creation of a jig for its respective validation.

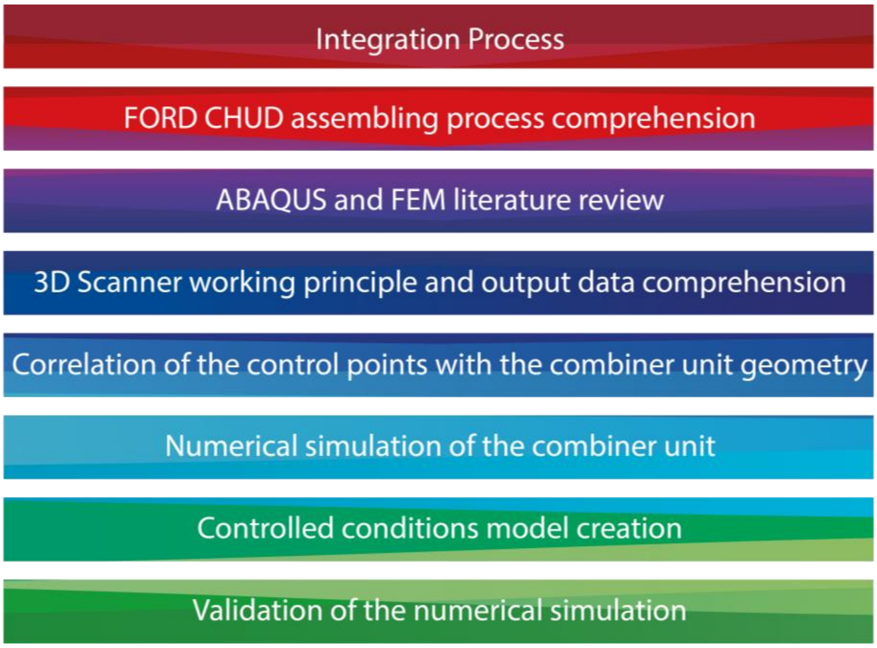

Figure 5: Flowchart

1.6 Structure

Apart from this chapter, this thesis is organized with eight more chapters:

- Chapter 2: Literature Review. A brief introduction to the Head-up Display mechanisms and respective variants as well as a short highlight on the part to be study – the Ford Focus CHUD.
- Chapter 3: FORD Focus CHUD. A more detailed description of the studied part, as well as some information on the building materials.
- Chapter 4: FORD Focus CHUD Combiner geometry deformation analysis. A deeper analysis to the main focus of this thesis is explained in this chapter.
- Chapter 5: ABAQUS CAE simulation model. The created simulation is described in this chapter as well as brief introduction to the theory behind the FEM method.
- Chapter 6: Jig development. The jig created in this work to replicate a controlled conditions model is explained throughout this chapter.
- Chapter 7: Validation of controlled model. Comparison of all the results obtained from different sources of testing and consequently validation of the simulation model.
- Chapter 8: Conclusions and Future Work: This chapter is based on the conclusions of the thesis project as well as future working perspectives;
- Appendix: Description of some other work performed during the internship.

2 Literature Review

This chapter resumes the technology advances in the automotive industry mainly on the user interface systems, like the dashboard and ultimately the HUD.

2.1 A briefing to the car and driver data transmission

Comparing a car interior from nowadays with a car from the 1930's, like the Ford Model A (Figure 6) shows us how much the car industry has evolved since day one. In fact, the first car produced didn't even had a speedometer, while as of present that would be unreasonable.

Figure 6: Ford Model A interior (Mecum, 2019)

With the advance of the car technology the information displayed in a car dashboard has been increasing through the years, firstly in an analogical way (Figure 7), where we would be able to have at least a speedometer, a rev counter and some info about oil and water temperatures as well as warning lights for the cooling system, the brake system and even for the battery.

Figure 7: Peugeot 205 GTi dashboard (Smith, 2019)

Despite the amount of data shown to the driver in an earlier past, the information passed on to the driver kept increasing and its becoming common for us to be presented with a digital dashboard, where apart from all the information we already had, we are now also able to analyze GPS and infotainment data (Figure 8). Considering the excessive amount of information and how it could be menacing the driver attention when driving there was a need to create some sort of device that would transmit the most important info and at the same time allowing the driver to focus on the road. Therefore, the Head-Up-Display was invented.

Figure 8: BMW dashboard (Roze, 2019)

2.2 Head-up Displays (HUD) and how they work

When driving its fundamental that the driver main focus be the road ahead of him which as we explained earlier doesn't really happen because of all the information the car transmits to us and we are forced to take our eyes from the road.

HUDs systems can project this information to the windshield at eye level, avoiding the driver to get the need to glance down at the dashboard for information. Despite sounding like a new technology, fighter jets have used a rudimentary HUD system since the 1950s to display data like altitude, speed and even targeting systems on the front of the cockpit canopy (Figure 9).

Figure 9: HUD in the aviation industry (Evans, 2019)

As for the automotive industry it's yet not so common to see this kind of systems despite having made its first appearance in a car in 1988 by General Motors. The two main variants we have in cars, when it comes to the image display are the traditional system, known by the windshield projection (Figure 10) and, more recently the projection in a transparent combiner, also known as Combiner Head-Up Display or simply CHUD (Figure 11). Even though this is a quite recent technology in the automotive industry that doesn't mean that it's only meant for high-end vehicles. (Neiger, 2012)

Figure 10: BMW HUD (Nicolazzo, 2019)

As a matter of fact, our analysis throughout this document will be done on the CHUD for the 2019 Ford Focus (Figure 11), a medium range car. Despite having a similar working principle as the HUD, the major difference comes in the components that make the two systems. A more detailed perspective of the CHUD technology is explained in the following chapter.

Figure 11: 2019 FORD Focus CHUD (FORD, 2019)

2.3 Combiner Head-up Display (CHUD) and how they work

The functioning principle of a CHUD is based on the same as the HUD, but instead of getting the image projected on the windshield, it is projected on a transparent polycarbonate or glass plate known as the combiner (assigned with a blue arrow in Figure 12). As a consequence, the combiner system is capable of creating a virtual image for the driver. As represented in Figure 12, the entire system is built of 3 major components: a PGU (Picture Generation Unit), the housing for the kinematics system, which is responsible for the combiner storage when the car is stopped and, at last, the imaging system.

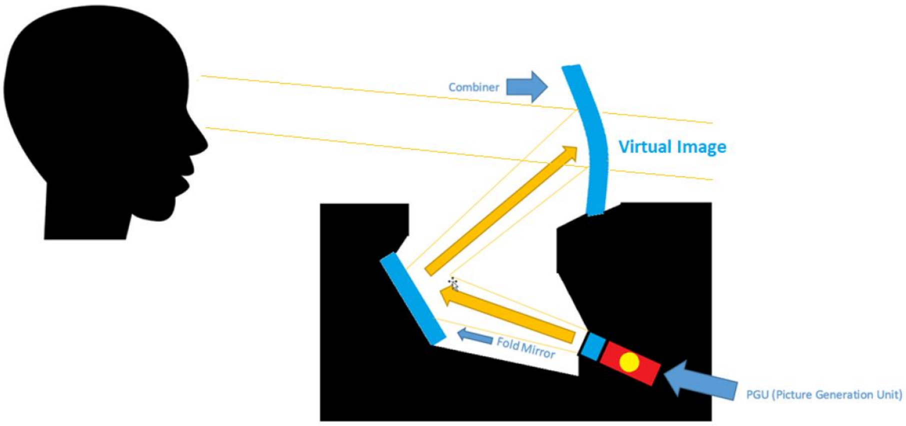

Figure 12: CHUD working principle (Almeida, 2019)

At BOSCH Car Multimedia Portugal, S.A. at the moment, the CHUD technology is being developed for two brands: BMW and FORD. Even though both CHUDs are based on the same working principle, they are slightly different when it comes to the assembly of the main components. These variations come in the combiner unit, the system responsible for the creation of the virtual image, while the rest of the CHUD mechanism is basically the same.

While both combiners are glued to their respective support, known as combiner support, the BMW CHUD also has an additional front cover with three complementary bolts that assure the correct fixation, as well as a firmer bonding of the combiner. This is clearly visible on Figure 13. The combiner is also tinted with a black color as a request from the customer.

Figure 13: BMW Combiner Unit

In the case of the FORD CHUD, the assembly process of the combiner with its support is done exclusively with the adhesive bonding. Opposite to the BMW CHUD the FORD CHUD has no tinted color, being totally transparent. This combiner unit can be observed in Figure 14.

Figure 14: FORD Focus Combiner Unit

After the assembly the combiner units are mounted into the kinematics system, responsible for its storage in the kinematic housing, which will make part of the entire CHUD system. Being an optical component, the dimensional stability of the component has to be close to perfection, so that image distortion can be avoided, among other problems related to image display.

For this work, the FORD CHUD will be the component to study, since the team is currently facing some issues regarding image quality rejection from the production line, due to the tight restrictions of the tolerances imposed by FORD.

3 FORD Focus CHUD

As previously explained the CHUD technology works based on a combiner unit, responsible for creating the virtual image for the driver to see. As for the FORD Focus CHUD, the combiner unit is composed of three main components:

- The combiner;
- The combiner support;
- The adhesive that bonds both parts.

An exploded view of these components, except for the adhesive layer is visible in Figure 15.

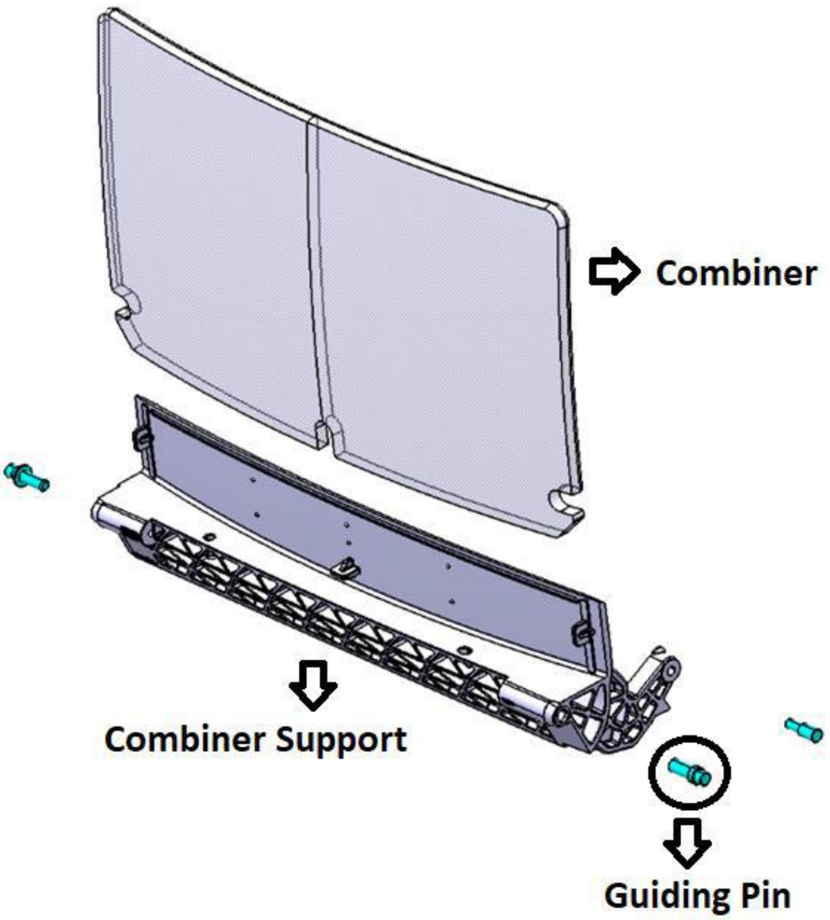

Figure 15: FORD CHUD Combiner Unit Exploded View (Almeida, 2019)

This is a sub-system of the bigger CHUD kinematics system, where the combiner unit is located, on the top, and can also be stored when it's retracted. The storage is assured by a cover that closes when the combiner is down. The cover can be seen in Figure 16, as well as the CHUD mechanism in its functioning mode, in other words, with the cover opened and the combiner in the display position.

Figure 16: FORD Focus CHUD

As previously stated, the combiner unit is the part to study of the FORD CHUD. This involves all the components that take part on its assembly. In order to understand the importance of each one and how they can influence the image quality, a closer approach to these three parts is done further ahead.

3.1 Combiner

The combiner in FORD Focus, represented in Figure 17, is the component responsible for creating the virtual image generated by the PGU to the driver. Being an optical component its manufacturing has to be done taking into account all the tight tolerances, otherwise the image in the combiner will most probably present some distortions. Other problem that may occur is the double image effect which can be caused by the incorrect shape or angle between both combiner surfaces.

Figure 17: FORD Focus combiner (McNamara, 2019)

The combiner is a free form component made from transparent polycarbonate (PC), which is also quite strong and resistant. Other materials can be chosen for the manufacturing of this part but PC was the one selected by BOSCH in partnership with FORD due to safety, in case of accident, and cost reasons. This part is achieved through injection and later subdued to a milling process in order to achieve its final shape as shown in Figure 18.

In order to assure the desired optical properties the combiner has a special surface treatment in the interior surface allowing the projected image to be reflected to the driver. Apart from this, it is also fitted with an anti-scratch coating.

Figure 18: FORD CHUD Combiner

Polycarbonate, also known as PC, is a dimensionally stable, transparent amorphous thermoplastic with a structure that allows great impact resistance. Polycarbonates features a working temperature range from -40 ºC to 130 ºC. This material is very demanding in applications that require transparency and high impact resistance, being a lighter alternative to glass and also a natural UV filter. Some examples of these applications are: aircrafts and aerospace components, automotive and electronic components and agriculture. The major disadvantage of polycarbonate is the fact of being very susceptible to scratching. Therefore, as said before it is fitted with a scratch-resistant coating layer for better protection.

One of the issues that BOSCH is facing right now, is the fact of these components coming out of specification from the supplier.

3.2 Combiner Support

As well as the combiner, this component is the result of an injection but, in this case, the used material is glass fiber reinforced plastic. The combiner support (Figure 19) is fitted with two guiding features on both side ends and, a third one responsible for the rotation of the combiner unit. This rotation happens due to the combiner support connection to kinematic system of the FORD CHUD, enabling the storage of the entire combiner unit.

Figure 19: FORD CHUD Combiner Support

The combiner support is the part responsible for supporting the combiner when they are bonded together with the adhesive. Besides the rotation and the storage, the guiding features are also responsible for keeping the combiner in the correct place with the right alignment.

Being the part where the adhesive will be dispensed and the combiner is glued it is mandatory that the dimensional precision of the combiner support meets the standards. Unfortunately, at the moment this part faces some difficulties in the injection process resulting in dimensional problems that will consequently alter the combiner surface leading to image distortion.

During the bonding process between the combiner and the support, to make sure the first one will be glued in the correct position the combiner support has some important features on its surface. From the position supports (one in the center and two on the sides) and the lateral pads to the spheres, which have a quite reduced size, all of them contribute to the correct positioning and shaping of the combiner.

The combiner support is made from glass fiber reinforced polyamide. Polyamides are crystalline polymers typically produced by the condensation of a diacid and a diamine. (McKeen, 2014) As an engineering plastic, polyamides are often compounded with glass fiber, pigments, fillers and toughening agents for the polymer to achieve specific properties. (Polymers, 2019)

Fiber reinforced polymer composites, or FRPs are subdivided into:

- Carbon fiber reinforced polymer composites (CFRPs);
- Glass fiber reinforced polymer composites (GFRPs);
- Aramid fiber reinforced polymer composites (AFRPs).

In every type the fibers are encased in a resin matrix, also known as the continuous phase.

Glass fiber is fabricated from silica (more commonly known as sand), sodium and calcium carbonates. These materials are taken into a furnace and heated to 1700 K. Later they are extruded directly from the furnace through metal orifices that can be found in different diameters in order to produce the filaments. A high speed winder revolving faster than the exiting molten glass draws them under tension into very fine filaments. (York, The Essencial Chemical Industry - Materials and Applications, 2013)

In Figure 20 it’s possible the influence of the increment of the fiber glass ratio in the polyamide. With 0% the polyamide is a ductile material, but as soon as it is reinforced with the fiber glass there is a significant increase in the mechanical resistance, shown by the tensile strength. The cost of this reinforcement is the loss of ductility.

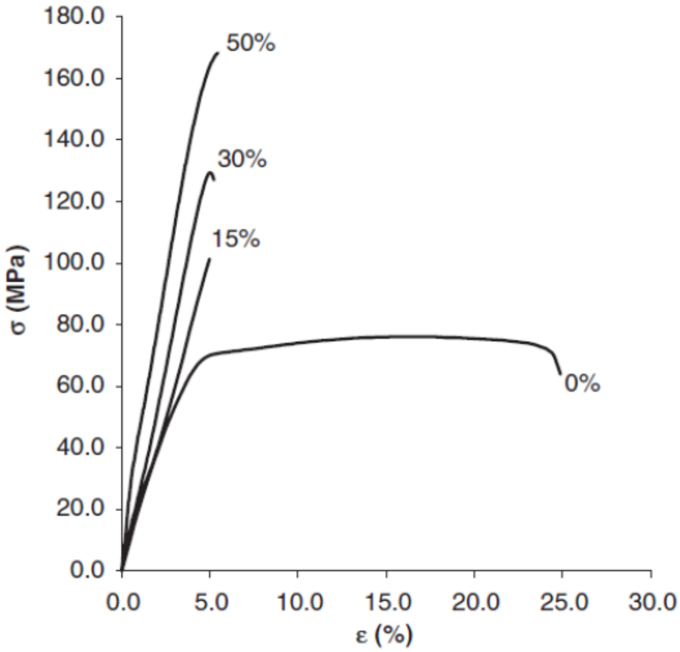

Figure 20: Influence of the glass fiber ratio at 20ºC (B. Mouhmida, et al. 2006)

In Figure 21 there is possible to see the effect the temperature can have on the polyamide with or without the glass fiber reinforcement. It’s clearly visible that the reinforcement of the polyamide brings positive results since the failure strain is constant and within the lower values (not more than 10%), while the non-reinforced polyamide has a high rate of failure as the temperature increases. Therefore the glass fiber reinforcement is very important since a car interior can reach up to 80ºC in summertime.

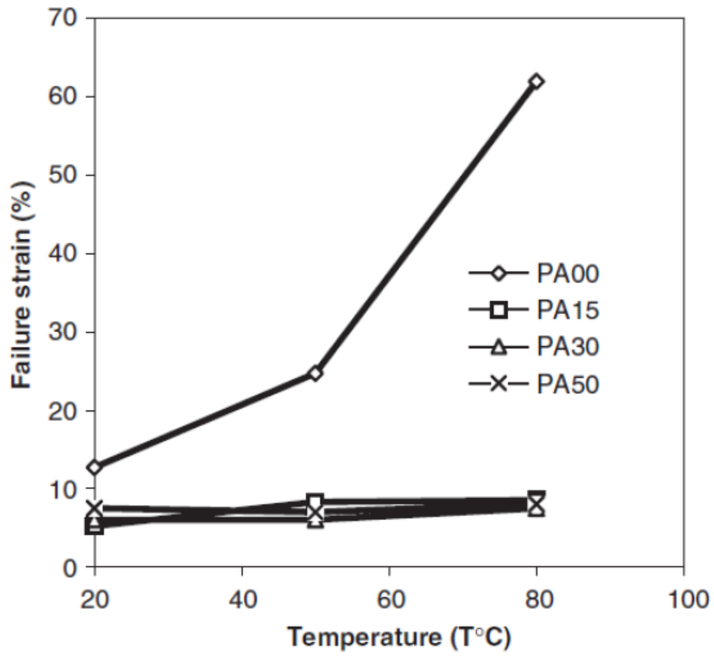

Figure 21: Temperature effect on the failure strain with different glass fiber ratios (B. Mouhmida, et al. 2006)

3.3 Adhesive

The combiner and combiner support are bonded together by a one-component modified epoxy resin. The epoxy is largely used in a wide variety of applications and are probably the most used family of adhesives because of several characteristics such as:

- Excellent mechanical strength;
- Excellent resistance to heat;
- Excellent resistance to chemicals;
- Excellent adhesive strength;
- Low curing contraction.

There are two types of epoxy adhesives, known as the one-part epoxy and the two-part epoxy resin. As stated previously the adhesive used to bond our components is a one-component, or one-part epoxy. The difference in the number of parts that compose the adhesive, affects directly the curing process, resulting in differences between the two kinds. While the one-component needs to be heated, with an UV light for example, the two-component (base agent and hardener) curing starts when both components are mixed. Both curing processes are illustrated in Figure 22 and Figure 23.

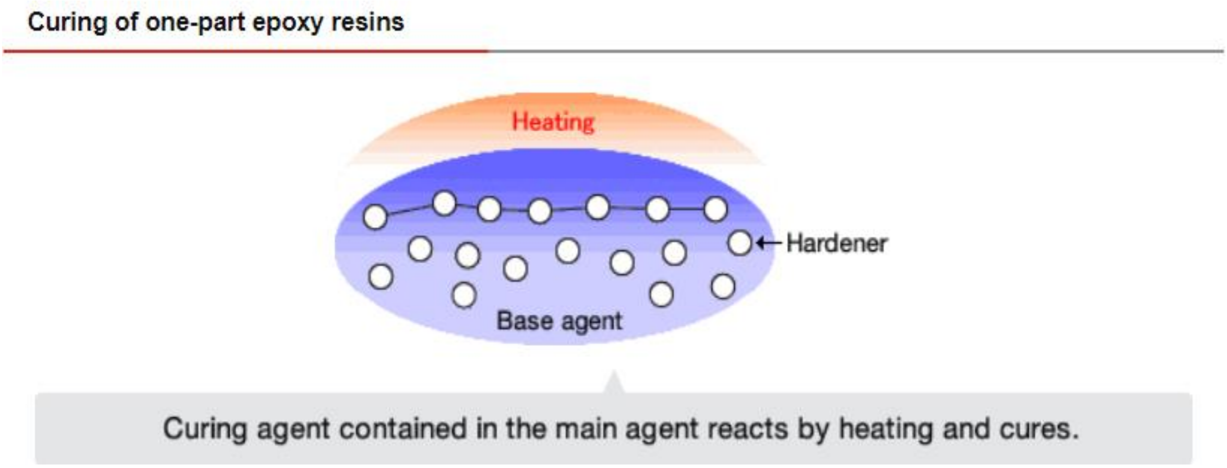

Figure 22: One-part epoxy curing process. (ThreeBond, 2019)

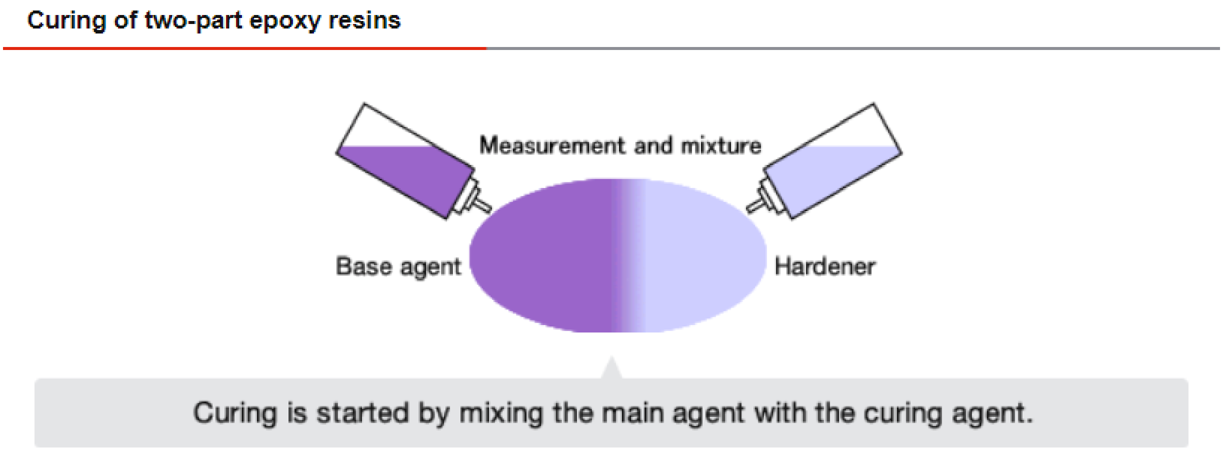

Figure 23: Two-part epoxy curing process. (ThreeBond, 2019)

Some highlights of the used epoxy resin are the service temperature range when cured of -40 ºC to +150 ºC, its suitability where application control is needed due to its fluorescence, the appliance by dispensing and the storage in containers at no more than 25 ºC.

One disadvantage of the epoxy resin is it weak resistance to peeling. To counter this the epoxy resin is modified with the addition of a more tenacious polymer, called a modified epoxy resin like the one used in the bonding process of the combiner unit. One of materials used for the modifications is rubber that allows for the epoxy to present a much higher resistance to peeling. The small particles of rubber act like barriers to the propagation of fissures. (Silva, 2007)

4 FORD Focus CHUD Combiner and Combiner Support analysis

During this chapter, we will take a deeper look to the overall geometric stability of the combiner unit, including a deeper analysis to both combiner and combiner support, as well as what factors can cause its deformation.

The main issue is related to both the combiner and combiner support and their geometric deviation when compared to the nominal dimensions. The root cause of this problems is in the parts that come from the supplier, that usually are out of specifications. When both parts are combined the tolerances that have to be respected tend to deteriorate even more. The gluing process, as well as the glue itself can also have a negative effect in the fulfillment of the requirements. All of the possible factors will be thoroughly analyzed during this chapters.

4.1 Combiner geometry analysis

In order to analyze the free form surface of the combiner, a 3D Scanner machine (3D-Shape SpecGAGE3D type L) which is installed in the optical lab of BOSCH. The combiner is setup in the 3D shape scanner like in Figure 24. The machine then uses two cameras, as shown in Figure 25 to retrieve all the data needed for the surface analysis of the combiner.

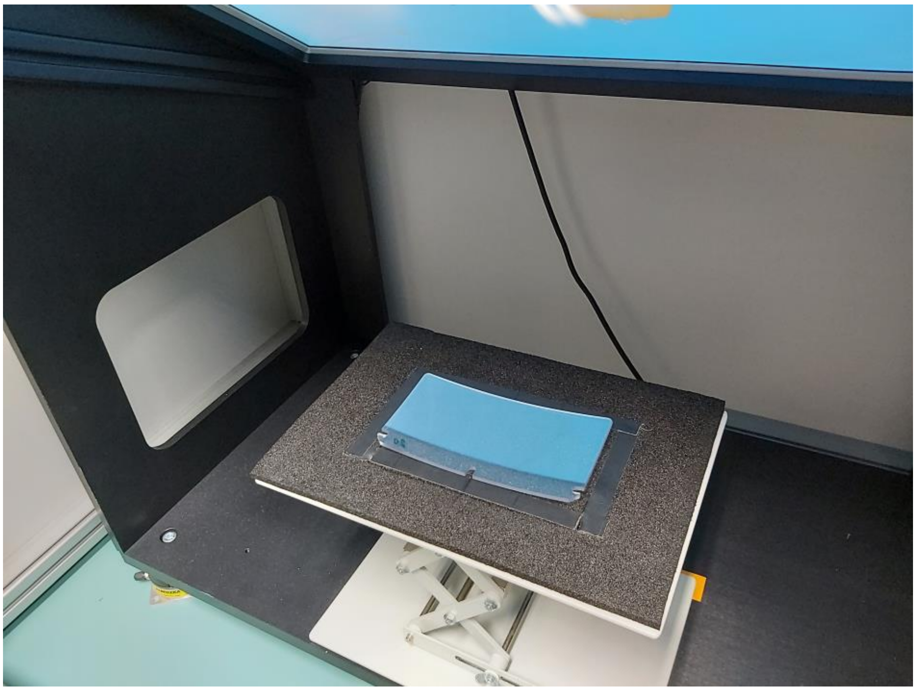

Figure 24: 3D Shape scanner machine

Figure 25: 3D Shape cameras

The output result is based on a color map that can tell if the part is curving more or getting flat. From the diagram in Figure 26 it’s easily comprehensible that the red and blue areas in the output of the 3D scanner, will correspond respectively to the flattening or increasing curvature of the combiner. Even so, a diagram like this will always be presented together with the output data.

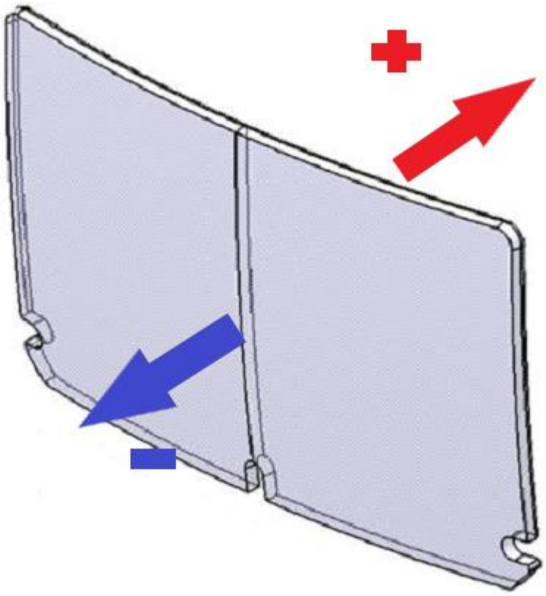

Figure 26: Scheme of the 3D scanner surface analysis

As for the output data from the 3D scanner machine of the combiner analysis, the result is shown in Figure 27. It is important to note that all the measures done in the 3D scanner are deviations of the real surface comparing with the nominal measures. All units are in µm except for the combiner dimensions, which are represented in mm. The dimensions located in the upright corner are in 1/m. Observing Figure 27 and keeping in mind the diagram of Figure 26, the conclusion is that the combiner is more flat than the nominal standard.

The PV value represented in Figure 27 is also known as Peak-to-Valley. This consists of a simple distance considering the lowest and highest of the measured height deviation when compared to the nominal height value. A diagram illustrating the measurement of this parameter is represented in Figure 28.

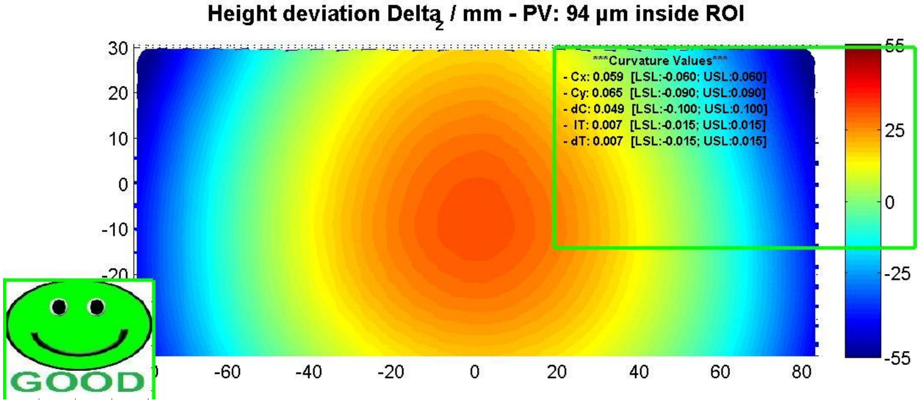

Figure 27: Combiner deviation to nominal before the gluing process

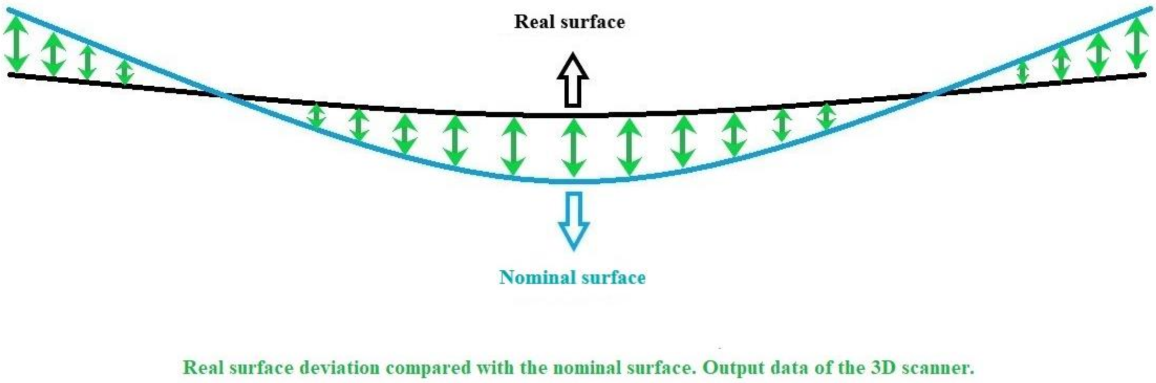

Figure 28: Working principle of the 3D Shape scanner

As visible in Figure 27, even before the gluing process there is already some shape variation relatively to the nominal values.

Even though combiners can be "GOOD" condition when coming from the supplier, like Figure 27 that was represented before, as soon as they are bonded together with the combiner support, the shape deviation of the combiner may be one of the factors leading to rejection in the production line.

Initially, 10 samples of combiners were measured in the 3D Scanner machine in order to choose the best 5 to be later taken to the production line and submitted to the gluing process. All the values are shown in Table 1 and are in µm. All these values are obtained with the 3D scanner and a Matlab code done by Bosch that takes the nominal CAD data and compares it with the studied part.

Table 1 – Combiner samples peak-to-valley deviation

Combiner	Peak-to-Valley Deviation
Combiner 1	117 μm
Combiner 2	137 μm
Combiner 3	170 μm
Combiner 4	138 μm
Combiner 5	128 μm
Combiner 6	158 μm
Combiner 7	149 μm
Combiner 8	188 μm
Combiner 9	170 μm
Combiner 10	168 μm

From Figure 29 to Figure 33 are the results obtained of the 5 selected combiners. They were selected according to the following:

- 1 combiner with the least deviation – Combiner 1;
- 1 combiner with the higher deviation – Combiner 8;
- 2 combiner with the same deviation value – Combiner 3 and combiner 9;
- 1 combiner with the closest value close to the average value – Combiner 2 (average value = 152.3 μm).

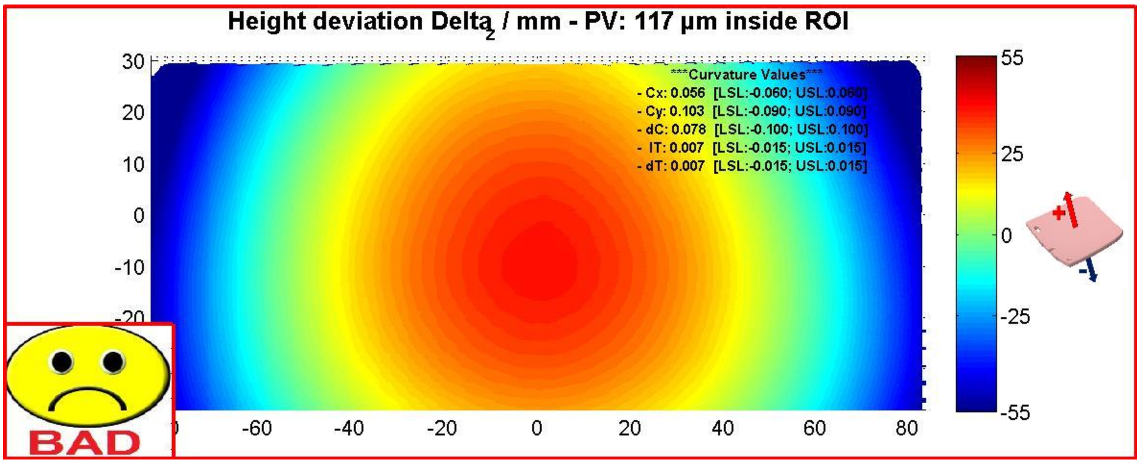

Figure 29: Combiner 1 before gluing

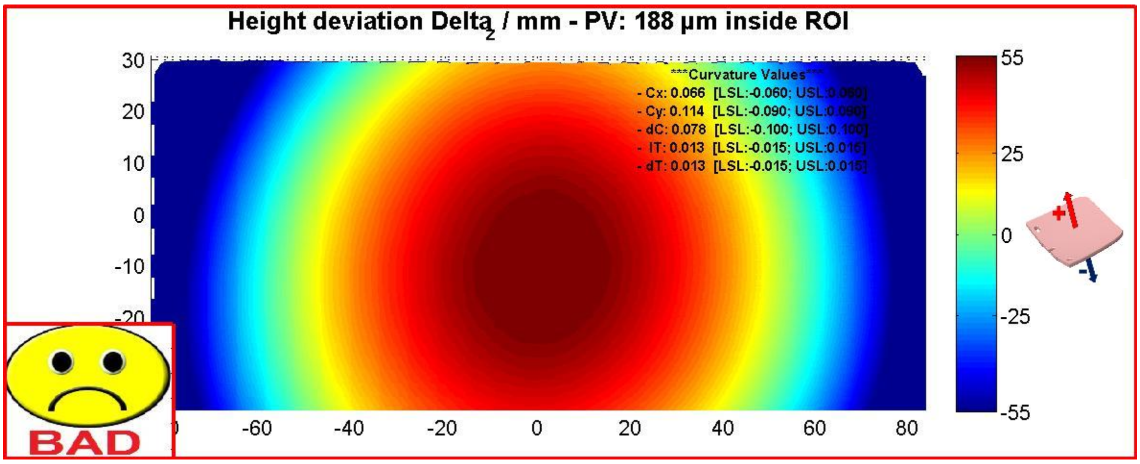

Figure 30: Combiner 8 before gluing

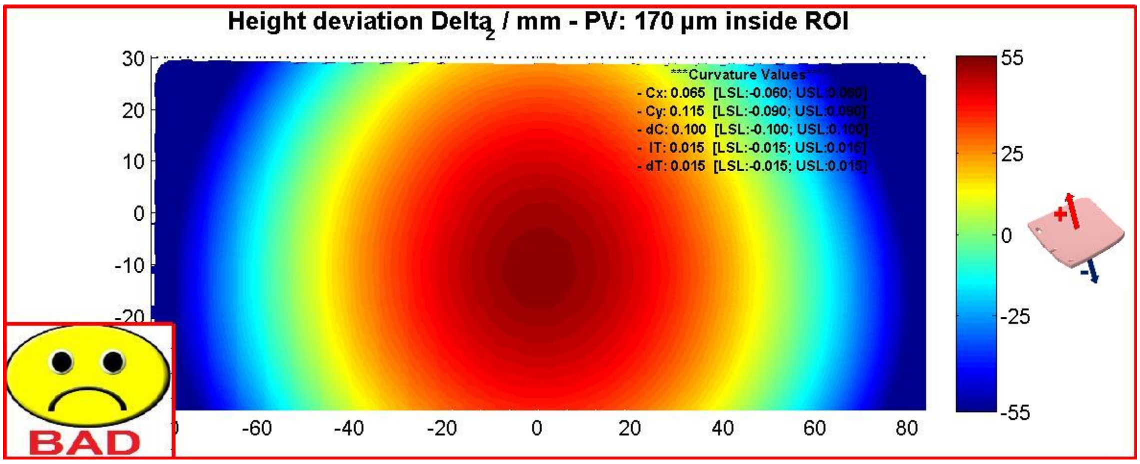

Figure 31: Combiner 3 before gluing

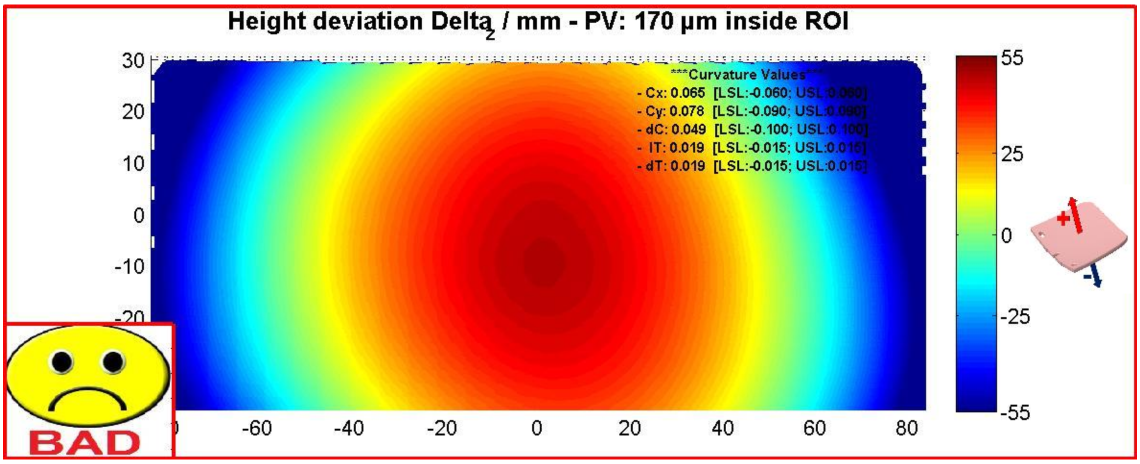

Figure 32: Combiner 9 before gluing

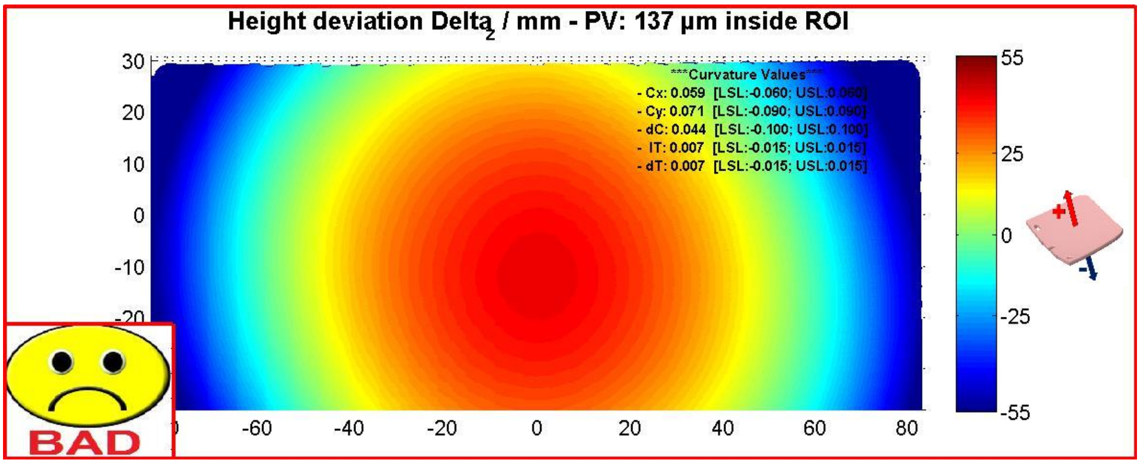

Figure 33: Combiner 2 before gluing

4.2 Combiner Support geometry analysis

In order to analyze the combiner support geometry several control points were chosen that were points already defined by Bosch. Inside these points we have two main groups: the P points and the M points.

On one hand, the P points are defined in areas where the part will contact with the combiner or, if not in contact because of the adhesive layer, will be very close to the combiner surface. On the other hand the M points are scattered through the surface in the adhesive-combiner support contact area. In Figure 34 the areas where the M and P points are located are identified.

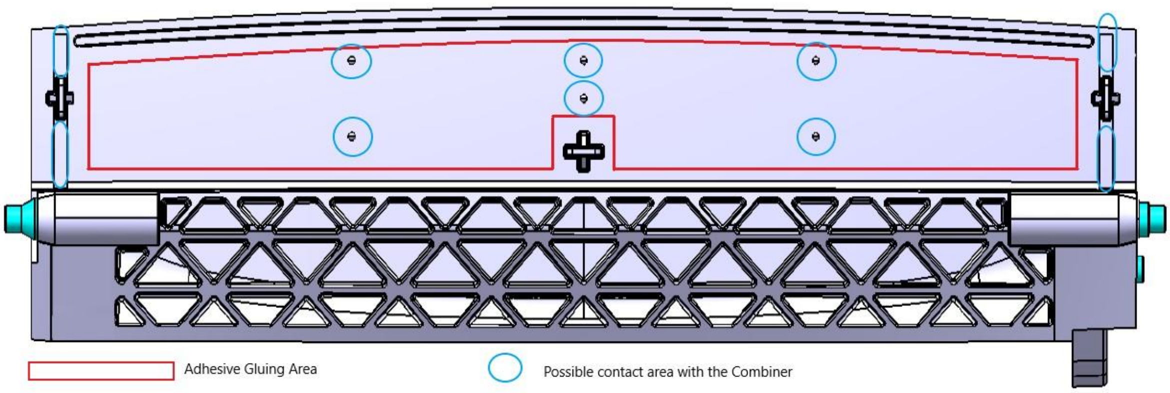

Figure 34: Combiner Support

For the study, a batch of 5 combiner support from the same series were selected and submitted to the metrology lab in Bosch for the M and P points' analysis. For confidentiality reasons the exact location of the measured points cannot be shown. Despite this, we will refer the contact points as the spheres, which are assigned with a blue circle and the pads or ribs as the parts also marked in blue but present only in the lateral part of the combiner support.

Since the combiner support is a part that is contact with the combiner, even though they have an adhesive layer in between, any deviation can be prejudicial to image quality of the combiner, since it can affect the combiner geometry. With the measuring of the combiner supports it's possible for us to study the control points and what effect they have in the combiner geometry. In Table 2 is possible to see the nominal data and also the upper and lower limit of allowed tolerances. All dimensions are in mm.

As for the measured values from point P11 to P16, in all measured combiner supports the values were out of specifications (Figure 35). It was also noted a slightly torsion of the combiner support, since there was a constant tendency for the same side of the part to be higher than the other. This tendency represents the existence of an asymmetry in the delivered parts from the supplier. This will be more visible later on after the gluing process analysis.

Table 2 – P points nominal measures and respective upper and lower limit

	Measurement description	Bench / Nº	Sample nº			
			Nominal	USL	LSL	Unit.
1	P2	25235	-4,19	0,05	-0,05	mm
2	P3	25235	-4,17	0,05	-0,05	mm
3	P4	25235	-4,18	0,05	-0,05	mm
4	P5	25235	-4,21	0,05	-0,05	mm
5	P7	25235	-4,19	0,05	-0,05	mm
6	P8	25235	-4,17	0,05	-0,05	mm
7	P9	25235	-4,18	0,05	-0,05	mm
8	P10	25235	-4,21	0,05	-0,05	mm
9	P11	25235	1,09	0,05	-0,05	mm
10	P12	25235	1,10	0,05	-0,05	mm
11	P13	25235	2,37	0,05	-0,05	mm
12	P14	25235	2,37	0,05	-0,05	mm
13	P15	25235	1,09	0,05	-0,05	mm
14	P16	25235	1,11	0,05	-0,05	mm

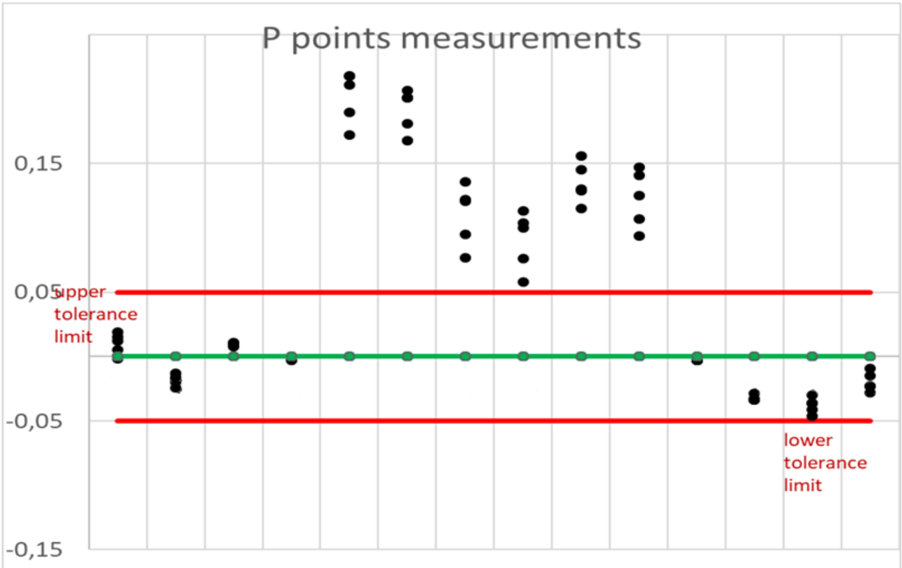

Figure 35: P points measuring output

4.3 Combiner Unit assembly process

After having the combiners measured in the 3D Shape scanner and the combiner supports in the metrology lab, the parts were taken to the production line in order to be bonded together. Previously to the combiners submission in the gluing machine, these are cleaned with a compressed air pistol to avoid any impurities in the bonding area and so assure a good quality adhesion.

As represented in Figure 36, the combiner as some guiding cuts to allow the correct positioning of this component in the combiner support during the gluing process. The area in blue represents the gluing area, which is where the adhesive layer will be bonding the combiner to the combiner support.

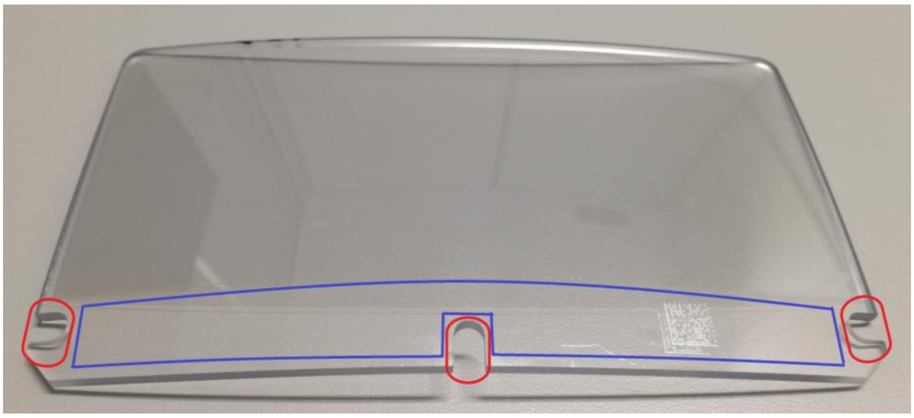

Figure 36: Combiner gluing area (blue) and guiding cuts (red).

While the combiner has the guiding cuts, the combiner support has guiding pins. These pins is where the guiding cuts will fit.

At a first stage in the gluing process, the combiner support enters the glue dispensing machine and has the glue dispensed on its surface. Once dispensed, the combiner support exists the machine, allowing the operator to manually place the combiner on top of it. For these stage, the glue is liquid and the operator only has 20 seconds to place to complete the task. If not done in the required time, the glue can lose essential properties, resulting in a bad adhesion that can lead to future delamination.

Having the task done, it means both components are placed together with the liquid adhesive layer in between. The following step is the automatic introduction of the parts in machine, but this time to cure the adhesive. For confidentiality reasons the curing method cannot be specified.

Once cured, the resultant component is called combiner unit.

4.4 Combiner Unit geometry analysis and typical problem

In order to continue our study, the combiner unit is then analyzed in the 3D Scanner. This way we will be able to see what deviations can happen as a consequence of the bonding process, the glue itself and the fact that the components were out of specification.

In Figure 37 it’s possible to see how the combiner unit is setup into the 3D scanner.

Figure 37: Combiner unit analysis on 3DShape Scanner

The glued combiners analyzed in the 3D shape scanner are shown from Figure 38 to Figure 42. The glued combiners are in the same order as in chapter 4.1.

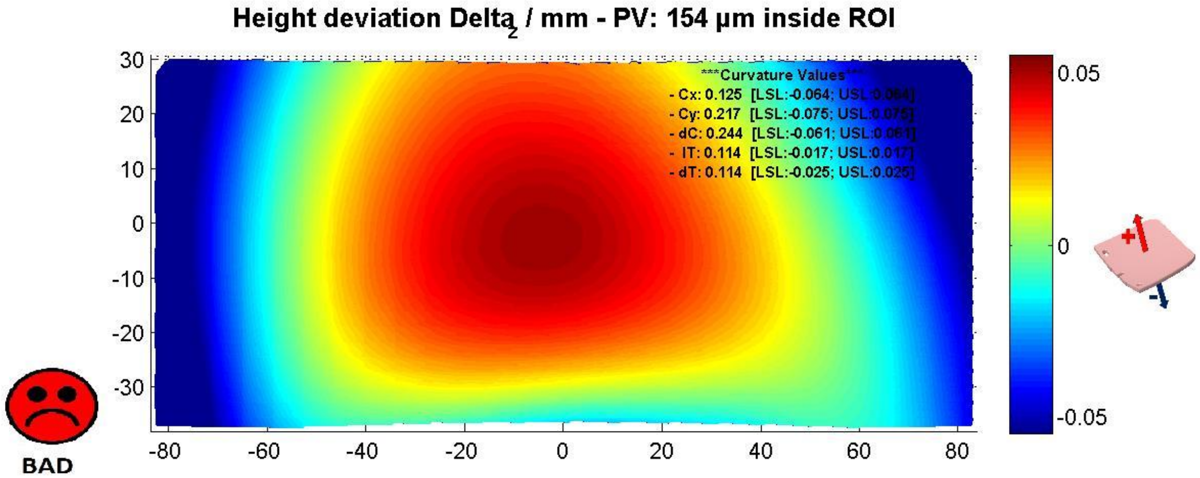

Figure 38: Combiner 1 after the gluing process.

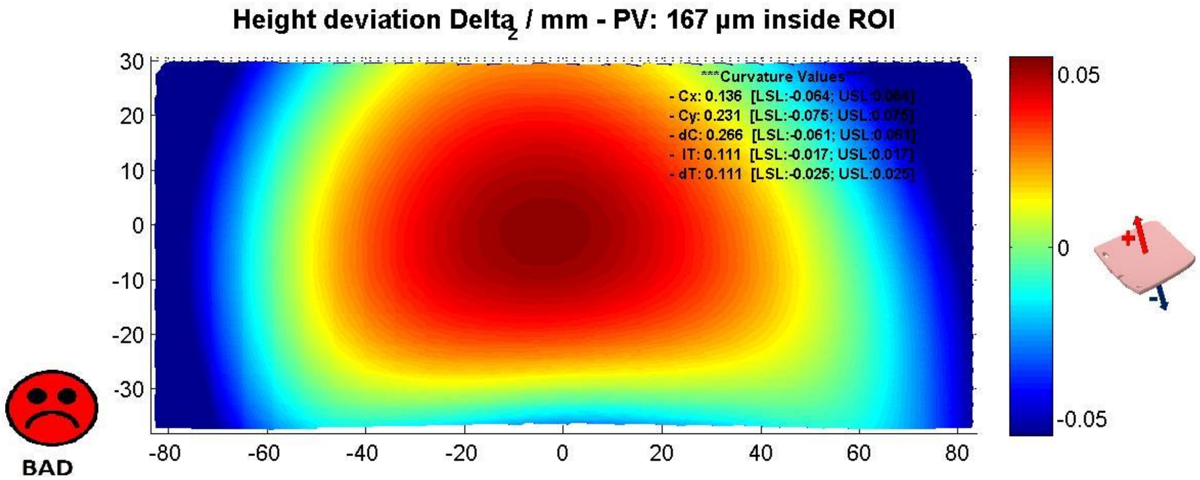

Figure 39: Combiner 8 after the gluing process.

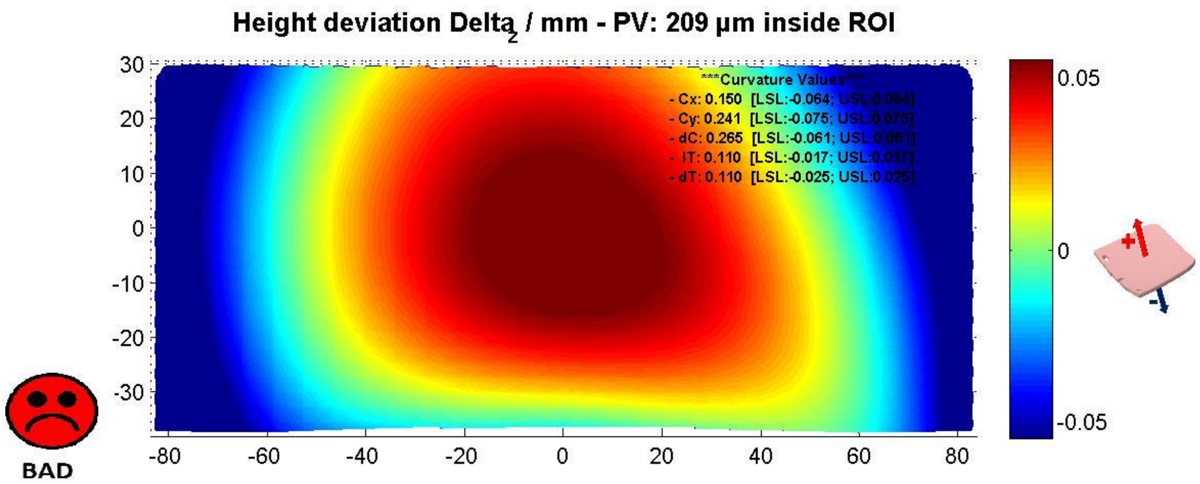

Figure 40: Combiner 3 after the gluing process.

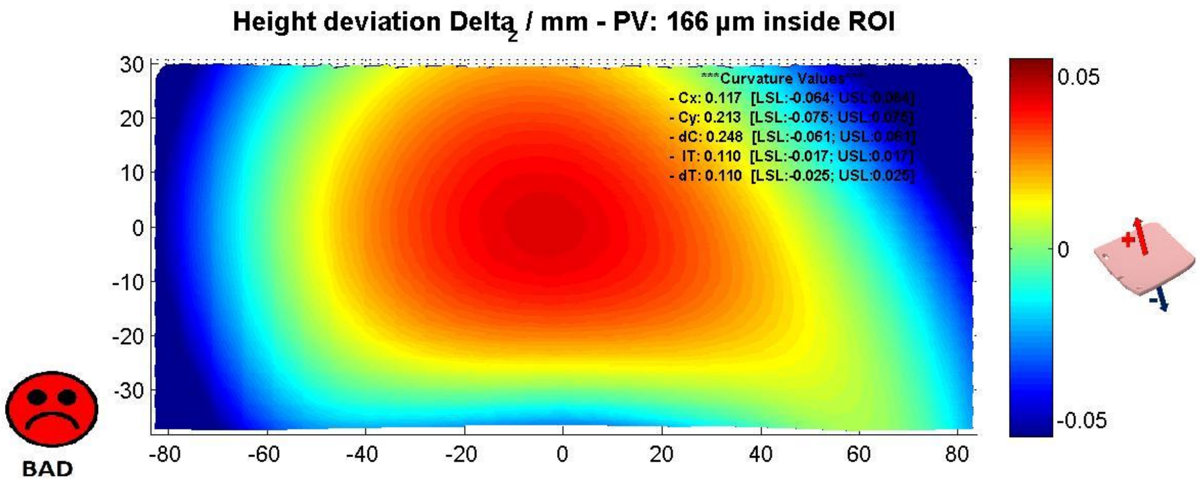

Figure 41: Combiner 9 after the gluing process.

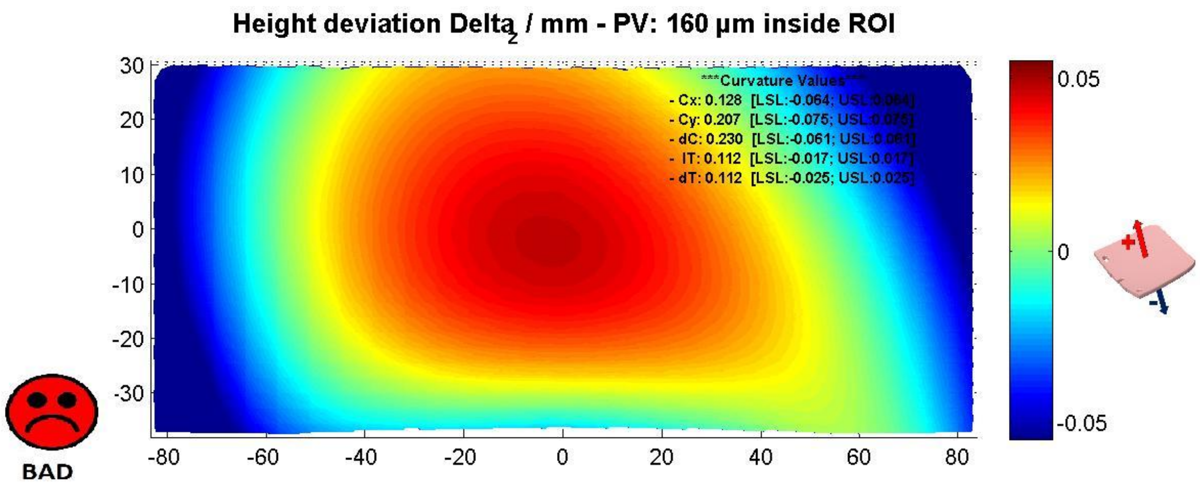

Figure 42: Combiner 2 after the gluing process.

From the obtained images we can clearly understand that all the combiners suffer some sort of deviation mainly to the right side. This shows the effect of the combiner support asymmetry referred, the out of tolerances control points and the initial deviation of the combiner.

Although it might not be clear what the root cause for the combiner unit deviation is, the possible assumptions done are:

- The component can already come with a slight torsion from the manufacturer, resulting in the side deviation and asymmetry, as well as the higher measured values. Being an injected component it's hard to have an accurate dimensional part, since the tolerances are in µm;
- The spheres, because of being all out of specification, represented in red in Figure 43 can also be the cause of the deviation;
- The ramp shape of the pads as well as the different heights in both sides. Analysing the table on Figure 43 and considering that from P2 to P5 we have one pad, and from P7 to P10 we have another one is visible the difference between them. Now, considering that the pair P2 and P3 and the pair P4 and P5 correspond, respectively to the bottom and top part of the same pads, it's easy to observe the ramp phenomenon happening in each part of the pad.

	Measurement description	00420968613011264 0000133918		00447778613011264 0000133918		00447788613011264 0000133918		00447798613011264 0000133918		00447818613011264 0000133918	
		Real value	Dev.	Real value	Dev.	Real value	Dev.	Real value	Dev.	Real value	Dev.
1	P2	-4,171	0,019	-4,178	0,012	-4,175	0,015	-4,185	0,005	-4,192	-0,002
2	P3	-4,183	-0,013	-4,188	-0,018	-4,186	-0,016	-4,190	-0,020	-4,194	-0,024
3	P4	-4,170	0,010	-4,172	0,008	-4,171	0,009	-4,169	0,011	-4,170	0,010
4	P5	-4,211	-0,001	-4,212	-0,002	-4,213	-0,003	-4,212	-0,002	-4,212	-0,002
5	P7	-4,218	-0,028	-4,213	-0,023	-4,213	-0,023	-4,205	-0,015	-4,199	-0,009
6	P8	-4,216	-0,046	-4,206	-0,036	-4,211	-0,041	-4,206	-0,036	-4,200	-0,030
7	P9	-4,214	-0,034	-4,209	-0,029	-4,213	-0,033	-4,214	-0,034	-4,213	-0,033
8	P10	-4,213	-0,003	-4,213	-0,003	-4,213	-0,003	-4,212	-0,002	-4,213	-0,003
9	P11	1,280	0,190	1,262	0,172	1,301	0,211	1,308	0,218	1,308	0,218
10	P12	1,281	0,181	1,268	0,168	1,301	0,201	1,307	0,207	1,301	0,201
11	P13	2,465	0,095	2,447	0,077	2,492	0,122	2,506	0,136	2,491	0,121
12	P14	2,446	0,076	2,428	0,058	2,474	0,104	2,483	0,113	2,470	0,100
13	P15	1,197	0,107	1,184	0,094	1,220	0,130	1,231	0,141	1,215	0,125
14	P16	1,239	0,129	1,225	0,115	1,257	0,147	1,266	0,156	1,255	0,145

Figure 43: Combiner support measured values

Apart from the assumptions done before, another possible cause for the deformation can be the thickness of the adhesive layer. As standard it should be 0.5mm across the entire gluing area. In order to analyze this situation some combiner units were picked to be submitted to a deeper analysis.

4.5 Adhesive thickness testing

This study was done to observe if the adhesive layer, after the cure, was matching with the specification of 0.5mm of thickness. If not it could mean the adhesive could be one of the causes for the deformation of the combiner.

To accomplish it, four combiner unit samples were picked and cut with a band saw cutting machine like in Figure 44. While two of the samples were cut through a line that passed through the upper spheres in the combiner support in a horizontal way (Figure 46), the other two samples were cut in a vertical way (Figure 47).

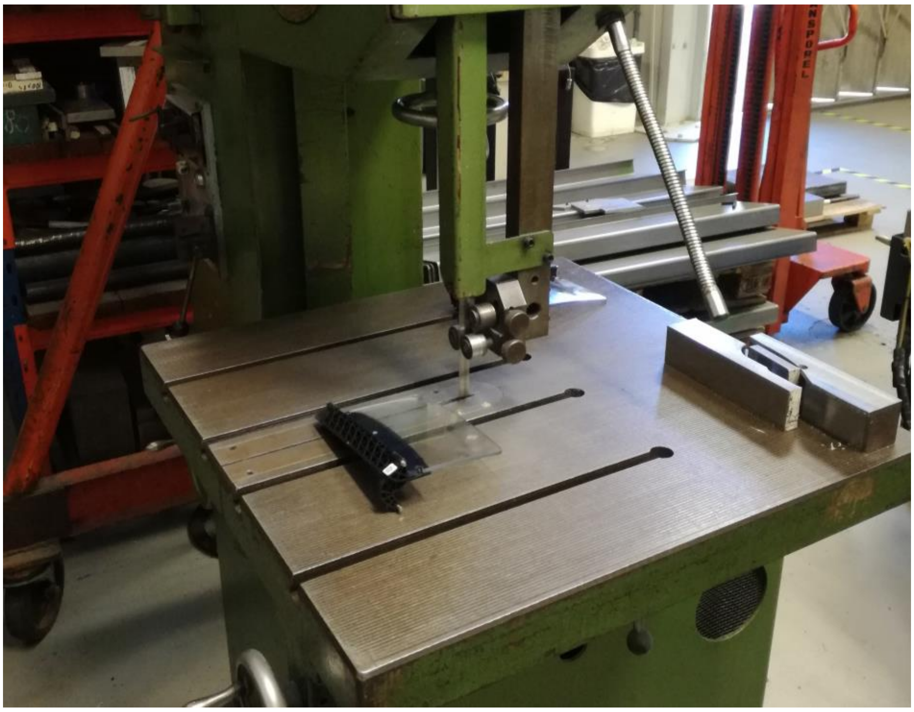

Figure 44: Band saw machine at FEUP

After the band saw machine the samples were reduced to small parts, containing the gluing area that was requested to observe. The samples are then submitted to a polishing machine, Struers RotoPol-21 (Figure 45), in order to attain a surface that can be properly analyzed in a microscope.

Figure 45: Polishing machine Struers RotoPol-21 at FEUP

The disks containing the sandpapers rotate at 300 RPM, which allows a good polishing of the surface. The final result is visible on Figure 46 and Figure 47.

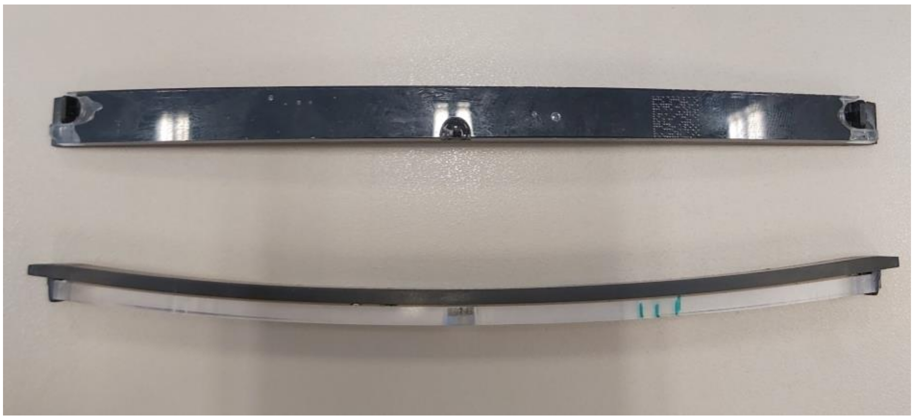

Figure 46: Combiner samples cut horizontally after the polishing process

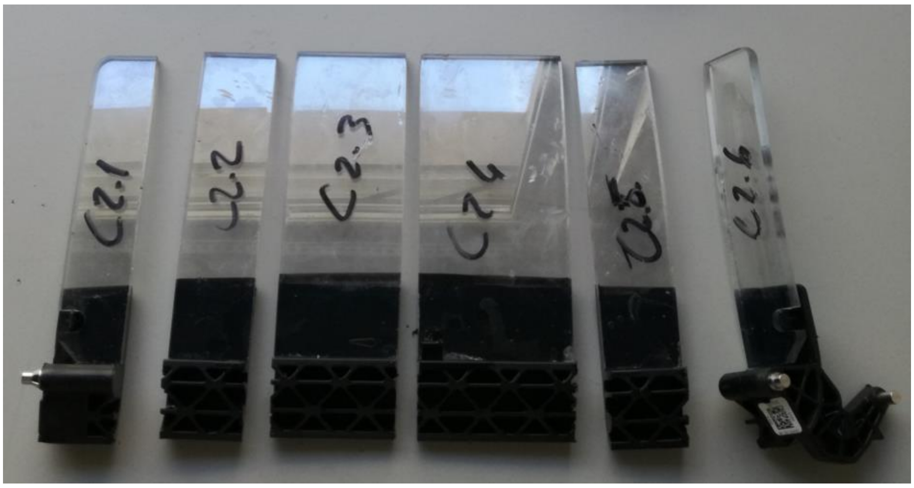

Figure 47: Combiner samples cut vertically (C2.1 on the left and C2.6 on the right)

The samples were measured in the INEGI (Institute of Science and Innovation in Mechanical and Industrial Engineering) lab after the polishing process. For the measures of the adhesive thickness was used an Olympus PMG3 microscope together with an image acquisition software named Olympus DP-soft.

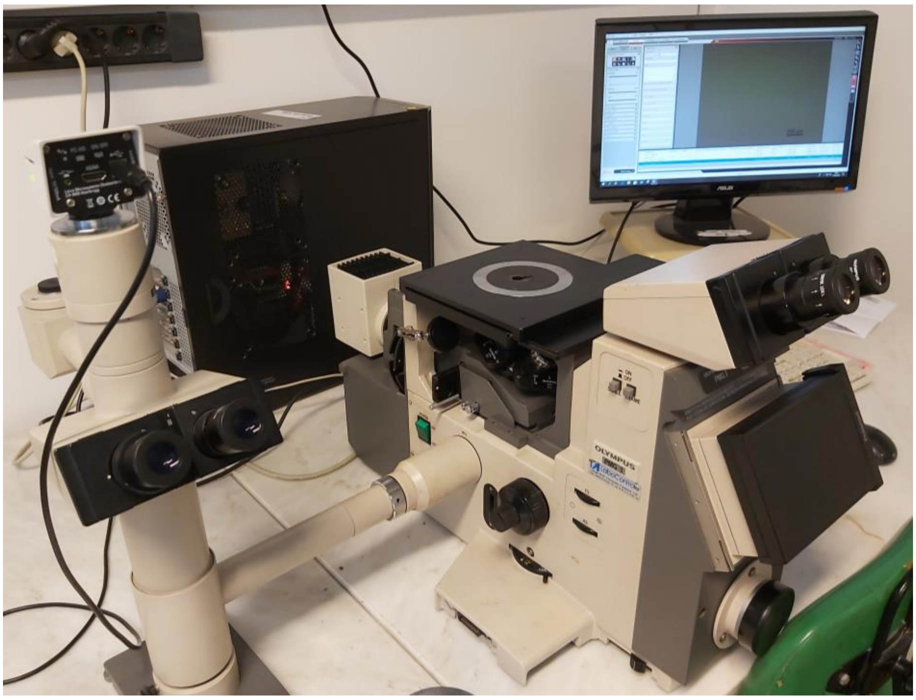

Figure 48: Olympus PMG3 microscope

Having samples that were cut in either a horizontal or vertical way, different points of analysis were selected. From Figure 49, it is possible to visualize the chosen method. In each measured point, three measures are done.

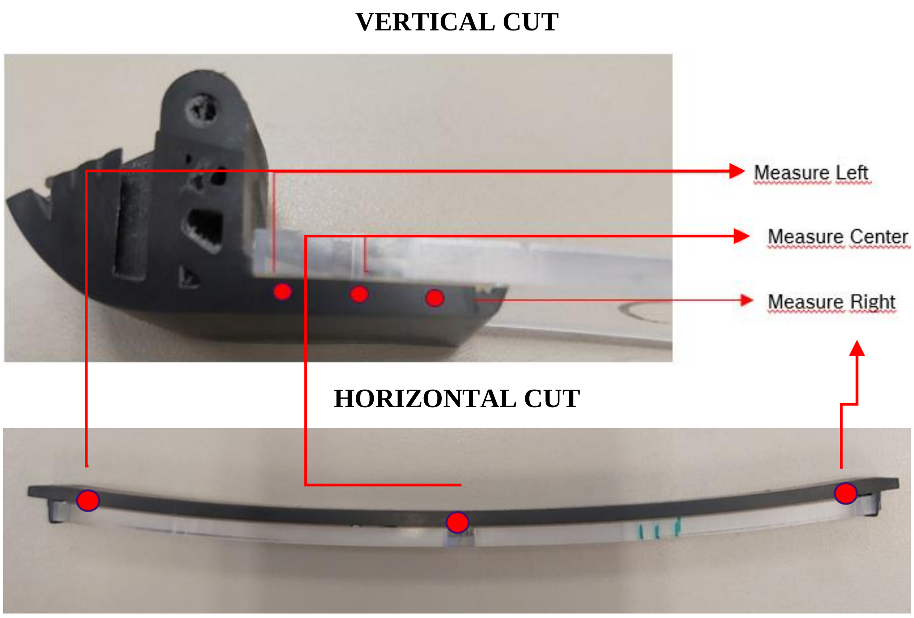

Figure 49: Chosen measuring points in both types of samples

In Figure 50 it's represented a sample of how the measures were taken with the microscope. It's possible to see four measurement lines, knowing that the one with 500.154 µm is the reference for the 0.5mm, where the rest are the real values measured. The measures can be seen in the following Figure 50:

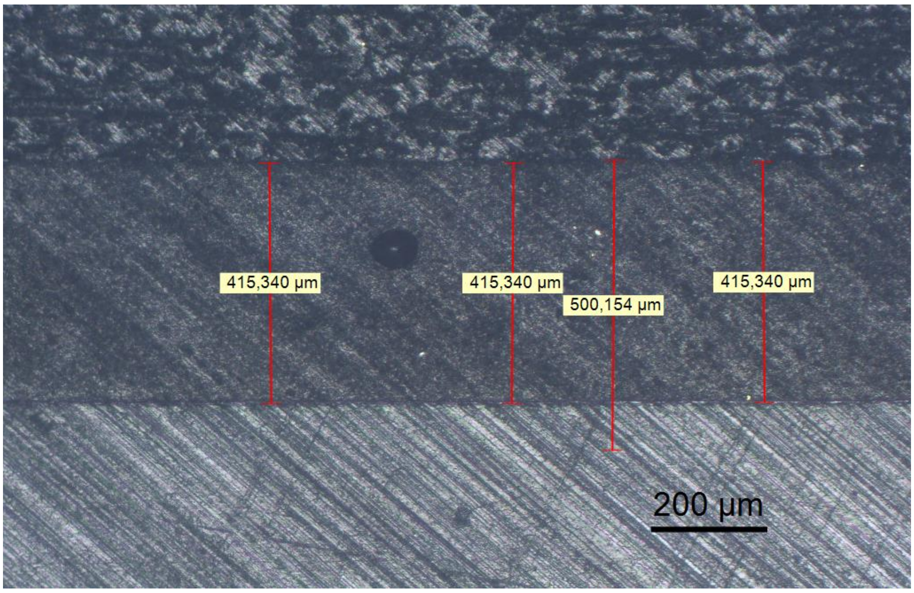

Figure 50: Output data from the Olympus microscope

Taking into account that there were 3 measuring points, a table with the results was created. The values presented are always the highest value measured in each point.

Table 3 – Measures from the combiners horizontally

Highest measured value	Measure 1 (Left)	Measure 2 (Center)	Measure 3 (Right)
Sample 1	489.824 µm	523.396 µm	507.599 µm
Sample 2	415.340 µm	531.296 µm	528.061 µm

Table 4 – Measures from the combiners cut vertically

Highest measured value	Measure 1 (Left)	Measure 2 (Center)	Measure 3 (Right)
C1.1	463.376 µm	420.872 µm	385.701 µm
C1.2	547.006 µm	493.245 µm	442.847 µm
C1.3	642.646 µm	599.649 µm	521.201 µm
C1.4	627.864 µm	601.135 µm	547.547 µm
C1.5	536.507 µm	512.423 µm	500.455 µm
C1.6	589.418 µm	583.681 µm	550.753 µm
C2.1	456.045 µm	432.072 µm	338.745 µm
C2.2	467.782 µm	419.406 µm	335.763 µm
C2.3	541.186 µm	541.175 µm	464.144 µm
C2.4	618.228 µm	551.061 µm	430.585 µm
C2.5	509.586 µm	539.200 µm	438.468 µm
C2.6	446.372 µm	464.148 µm	442.435 µm

It is clearly visible that the adhesive doesn’t maintain a constant thickness, as well as the values are far from the supposed 0.5mm or 500 µm, which can have a negative impact in the combiner geometry when bonded with the combiner support, resulting in one possible cause for the rejection of the combiner unit.

5 ABAQUS CAE simulation model

An ABAQUS CAE simulation model was created to try to forecast the combiner unit deviations considering the combiner support variations. The model created was simplified in order to allow a quick simulation time. This way, the adhesive influence is not considered. The creation and boundary constraints used in the simulation model are explained below.

5.1 Introduction to the Finite Element Method

The Finite Element Method (FEM) was introduced in the 1940s with the publication of a set of scientific papers, which described FEM as numerical techniques for finding approximate solutions to boundary value problems for partial differential equations. The basis of this method consists on a problem domain's subdivision into simpler parts, called the finite elements, and also on the calculus of variational methods to minimize an associated error function.

This method came to life as a need to solve complex elasticity and structural analysis problems in aeronautical and civil engineering. Apart from the different approaches made from the pioneers to this method, there is one common characteristic: mesh discretization of a continuous domain into a set of discrete sub-domains, usually called elements (Figure 51). Nowadays, FEA is used for several applications such as electromagnetism, heat transfer and fluid dynamics.

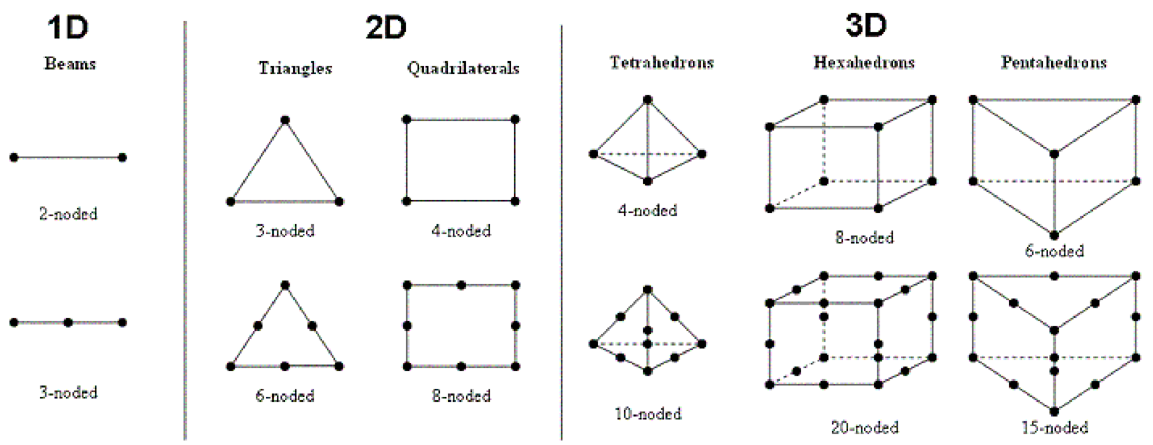

Figure 51: Elements Types (Andujar Moreno , 2019)

Product design using Finite Element Method (FEM) as largely expanded from the aeronautical and civil engineering to areas like biomechanical and automotive industry, because of the high profit it can bring since it allows the simulation of stiffness and strength of the materials as well as preventing unnecessary costs since there is no need to rely on a great amount of experimental tests. Using FEA analysis, we have the ability to develop any engineering structure design, test it and modified it in advance long before it reaches the manufacturing process of prototypes. Even when a product is already in the manufacturing process it can be optimized through digital format and then resulting in improvements in the manufacturing of it. To help attain an objective like this on this master thesis, ABAQUS CAE was the software chosen (Figure 52).

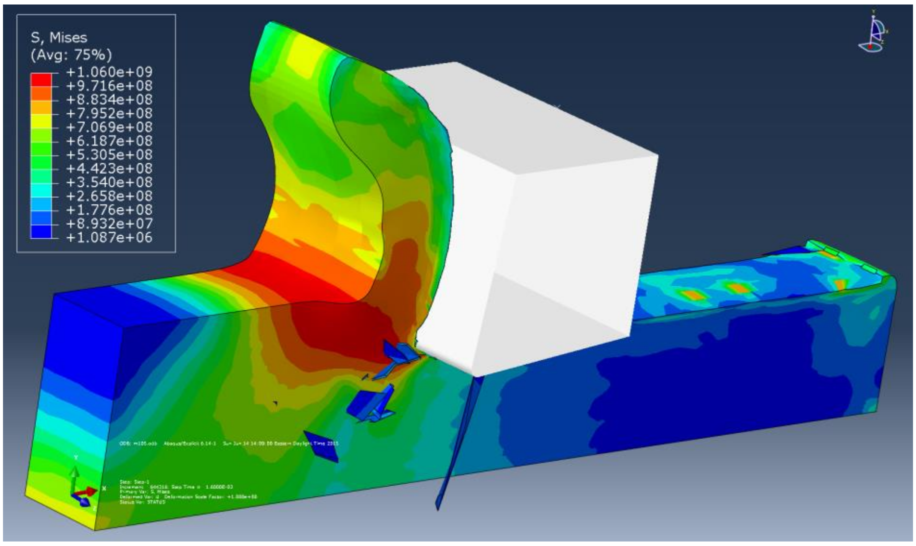

Figure 52: ABAQUS CAE Example (Ajri, 2019)

The FEA is the practical application of the FEM (Finite Element Method). It can be used to simulate cases related to heat transfer, structural analysis, mass transport, electromagnetic field and fluid flow.

In order to study any part or component the starting point is to define the material properties as well as assigning it to the respective part. The following step is to break down the part or component shape, be it complex or not, with unknown behavior into a system of points or the so called nodes. Their main function is to determine a mesh, which consists of a finite number of simple linear or geometric elements (Figure 53). These elements that subdivide the component shape will have a known structural behavior. With this done, the software will be able to compute the desirable output variables such as mechanical stress, mechanical vibration, fatigue among others. (GRAITEC, 2019)

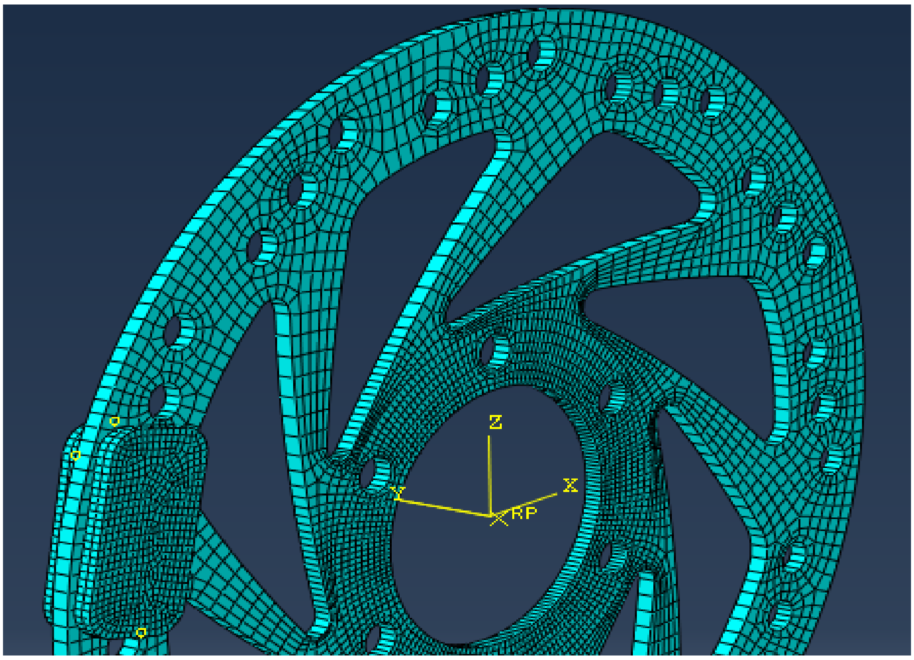

Figure 53: Brake discs mesh (adapted from Broekaart, 2019)

The FEA simulation also allows us to do either a qualitative or a quantitative evaluation, being the first one the quickest since there is no need for verifications in terms of values. As for a quantitative approach the values have to always be seen as an approximation to the real case scenario, since sometimes it's very difficult to transmit some variables into inputs in the ABAQUS CAE software.

5.2 Creation of the ABAQUS CAE model simulation

After the experimental tests it was clear that the combiner suffered deviations when glued. In order to have a better understanding of how the combiner behaves in this situation an ABAQUS CAE simulation model was created.

In a first approach for the creation of the model it was used the 3D combiner imported from CATIA V5, as shown in Figure 54.

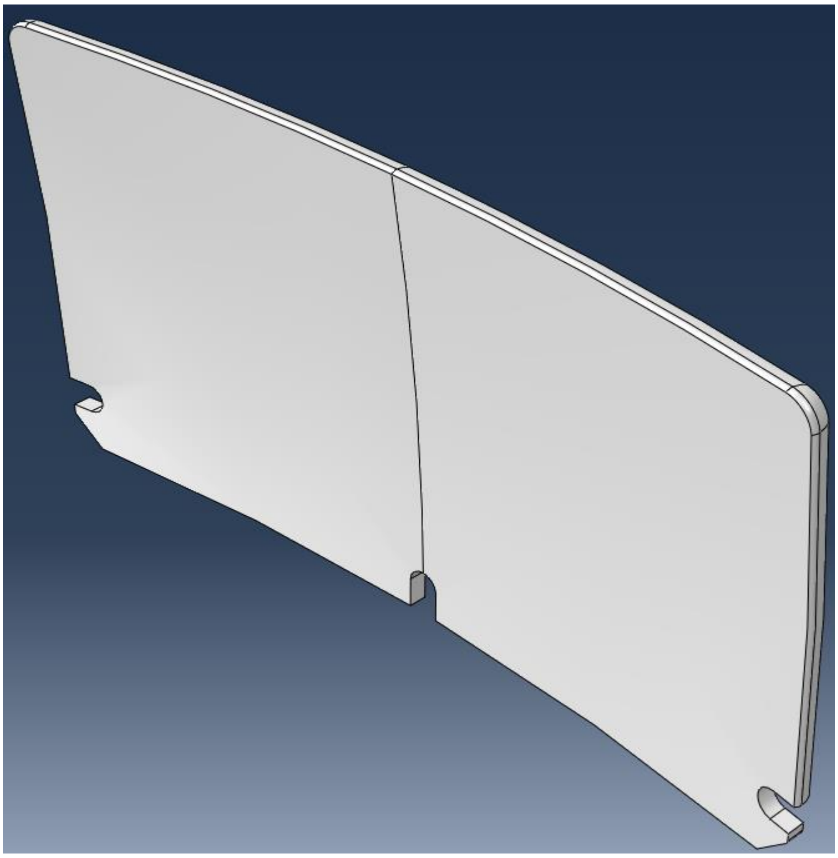

Figure 54: 3D Combiner part in ABAQUS CAE.

A first approach was done using solid elements. Still, this was soon abandoned since it was very time consuming, especially in the partitioning process, which allows a deeper analysis, that was taking around forty-five minutes to create a partition cell.

A countermeasure was the simplification of the part to a 3D shell element created from the middle surface of the original CATIA V5 part (Figure 55).

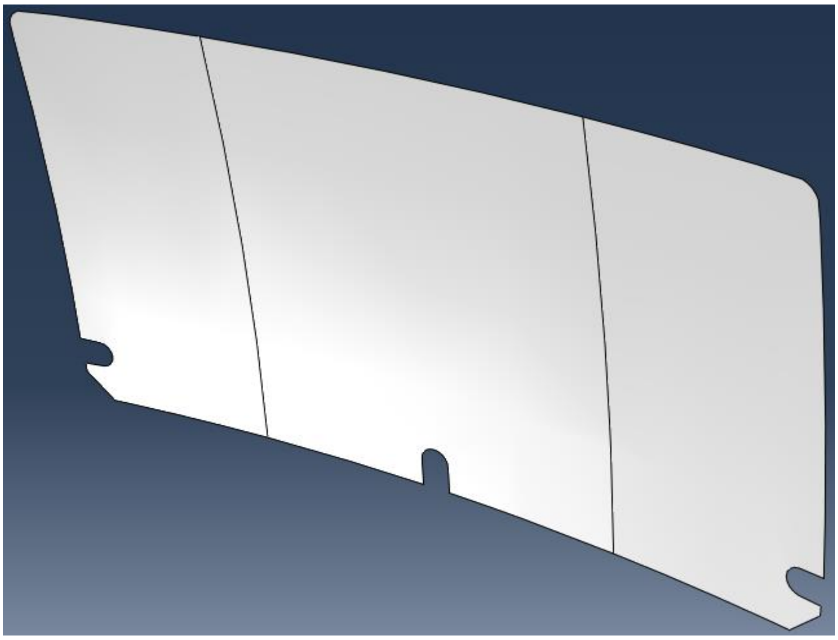

Figure 55: Combiner 3D middle surface in ABAQUS CAE.

In Finite Element Analysis (FEA) shell elements can be used for effective results. Since it allow the modelling of thin features with fewer mesh elements we can have a huge computational time saving. (Kuusisto, 2017) Despite this, shell elements are also easier to mesh and less prone to negative Jacobian errors which might occur when using extremely thin solid features.

So, using shell elements, a higher number of partitions were made on the part allowing the analysis of important surfaces or points we wanted to have a more precise output data (Figure 56).

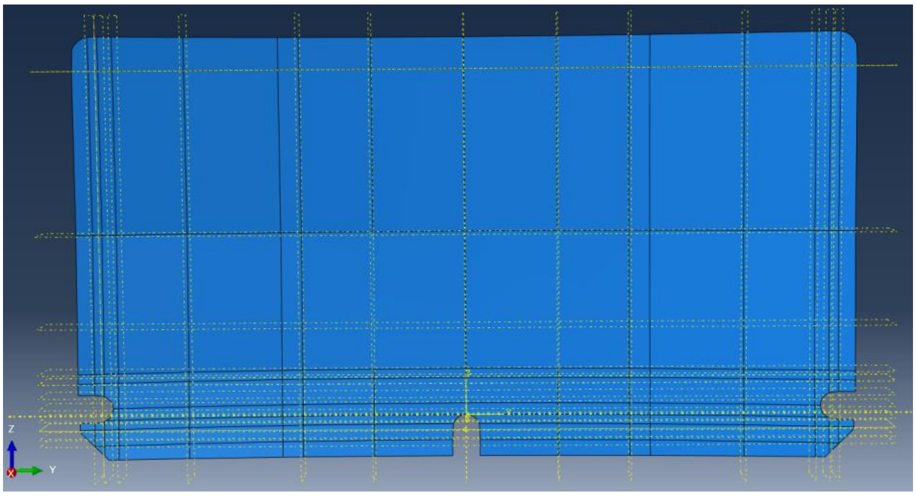

Figure 56: Combiner partitions.

The main purpose of these partitions, besides allowing the mesh to have a regular shape, was to create the references for the definition of the P points, known as the contact points between the combiner and combiner support. This way, it was possible to variate their displacement and study the consequences of the combiner, as if it would be attached to the combiner support.

As for the properties of the material, in this case the polycarbonate, the used data was a Young modulus of 2400 MPa and a Poisson coefficient of 0.42 (Figure 57).

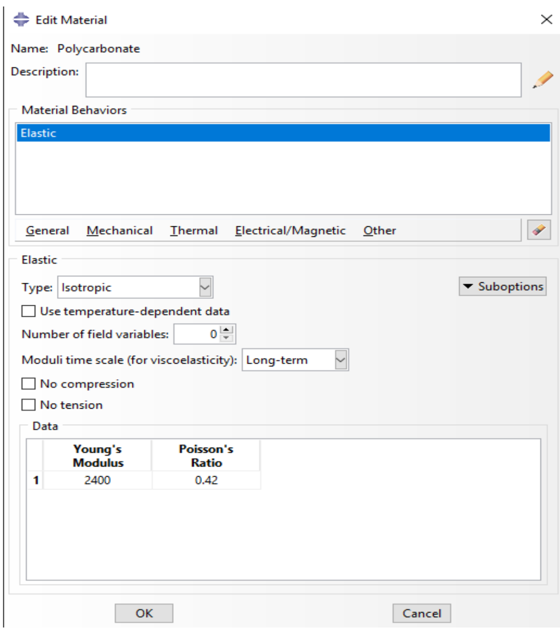

Figure 57: Polycarbonate properties submitted in ABAQUS CAE.

Boundary conditions is one of the most important steps to define. This was one the hardest steps when creating the model since the boundary conditions considering an adhesive bonding layer in a curved surface is not very straightforward. So, the boundary conditions set were divided in three areas, such as the gluing area, the guiding cuts and the P points displacement. As for the gluing area the restrictions (Figure 58) were the following:

- Displacement locked in the Y and Z direction;
- Rotation locked in X-axis and Z-axis;

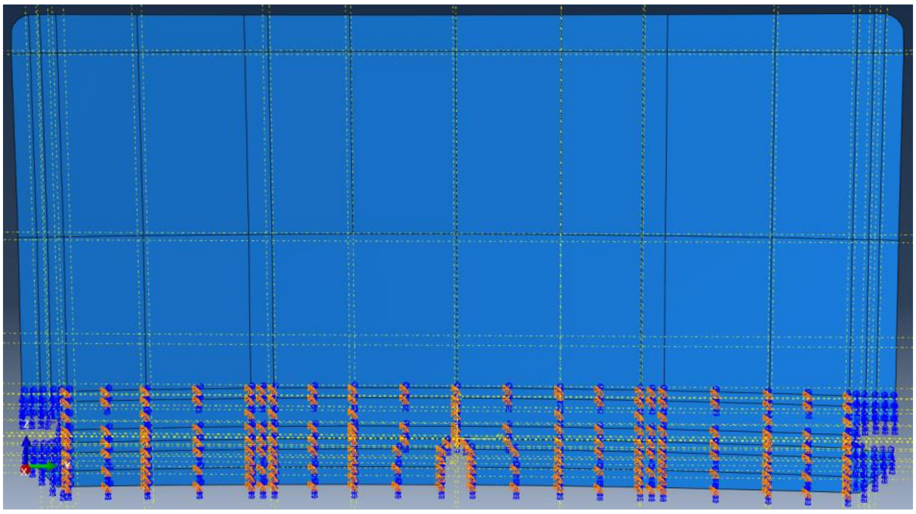

Figure 58: Gluing area boundary conditions.

As for the displacement in the guiding cuts, the boundary conditions set were the following:

- Displacement locked in Y-axis in the central guiding cut;
- Displacement locked in the Z-axis in the lateral guiding cuts.

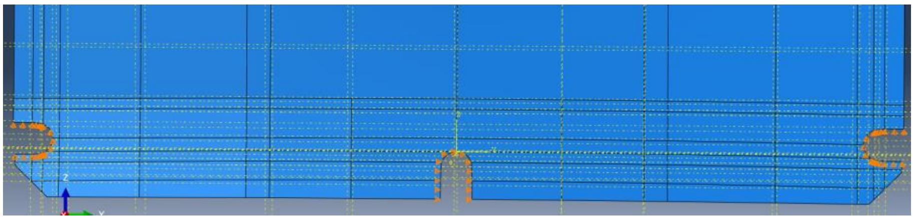

Figure 59: Combiner guiding cuts boundary conditions.

The P points are divided into the existing spheres in the gluing area and the pads on the lateral parts of the combiner support.

In the points P location, was set a displacement in the X direction that would correspond to the simulation of the behaviour of the combiner when glued, since these are the possible contact points. In Figure 60 is possible to see the location of these points. The spheres are assigned with a red circle while the pads are assigned with a yellow one.

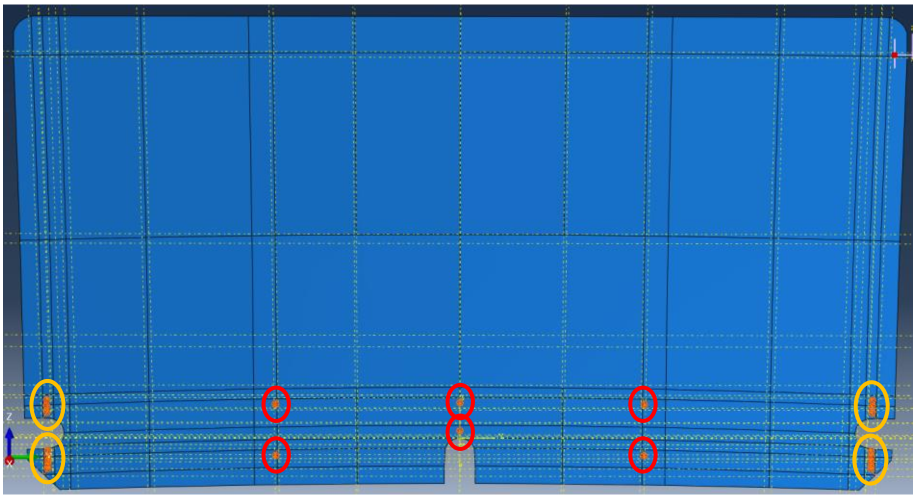

Figure 60: Displacement in the P points.

The displacement given to these points is based on the assumption that the P points are always in contact and the displacement value is based on the deviation when compared to the nominal measures.

As for the mesh, the inputs given were an approximate global size of 3mm, a maximum deviation control factor of 0.4 and a minimum size control by fraction of global size of 0.4. The element shape was Quad-dominated with the Free technique. The element type was the S4R: A 4-node doubly curved thin or thick shell, reduced integration, hourglass control, finite membrane strains. The meshed combiner is visible in Figure 61.

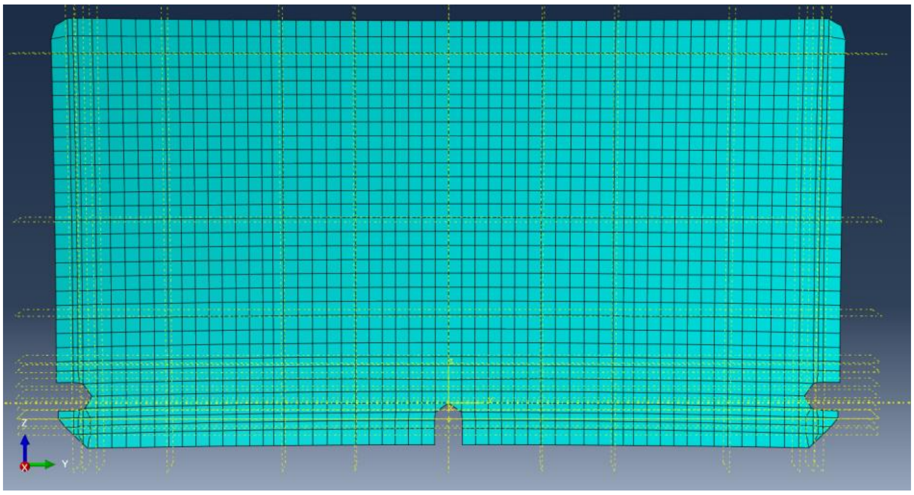

Figure 61: Meshed part

In a way to increase the resolution of the scale, it is possible to define the limits of it. This originates areas out of the limits of the scale, as shown in Figure 62 represented by the area in gray.

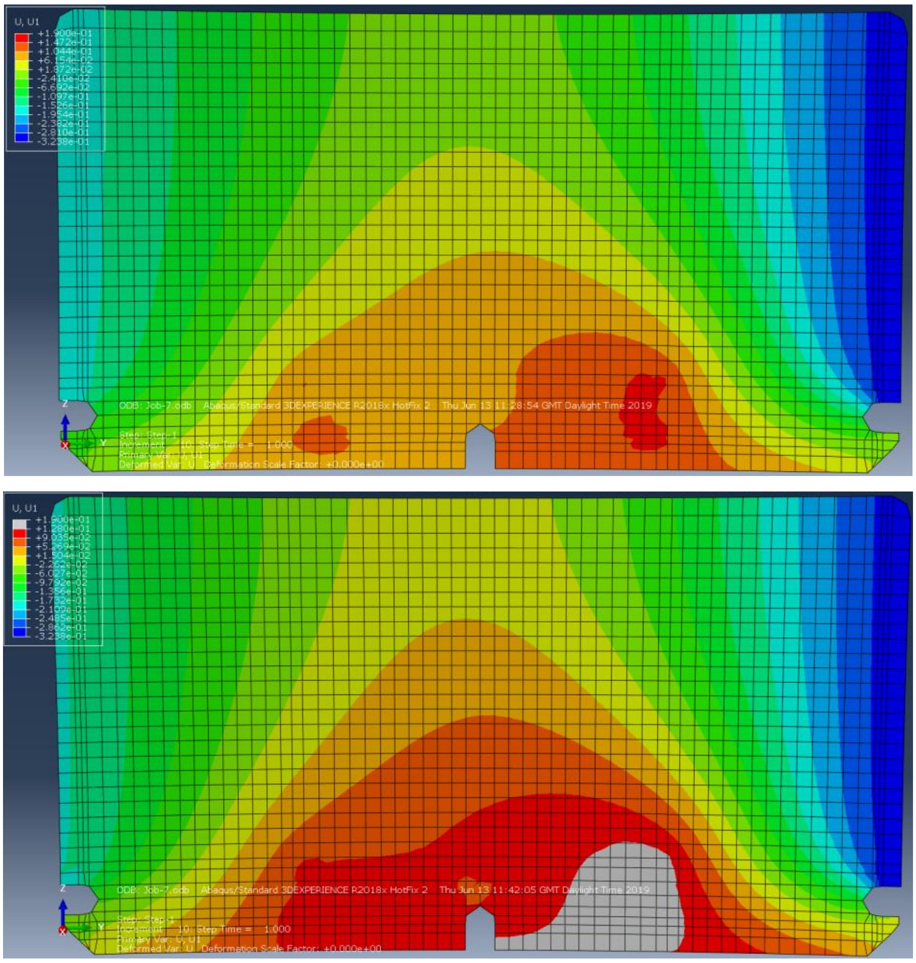

Figure 62: Simulation on the full area of the combiner

Based on the the combiners shown in the previous chapter a simulation was done to ensure the simulation was deforming according to the real part. Even though the simulation is done on the full area of the combiner shown in Figure 62, the important area to analyze is the one corresponding to the output of the mounted combiner measured in 3D scanner as represented in Figure 63.

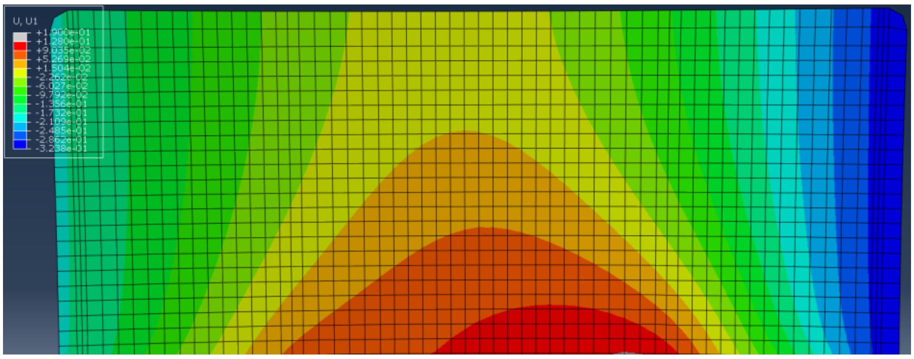

Figure 63: Analysis area of the combiner

In Figure 63 we a simulation done with the real deviation values measured from the combiner support that was glued with the combiner 2. Comparing it with Figure 42 there are some similarities when it comes to the right red curvature deviation and the color pattern in a red and yellow pattern in the center and blue in the boundaries of the combiner. Dizer que se usa os valores reis medidos no laboratorio de metrologia.

The real part has a more rounded deformation when compared to the simulation. The root cause to this scenario is the fact that in the simulation we are working with the nominal measures, also known as the nominal CAD, while the real component has, as identified in chapter 4.1 a different geometry when compared to the nominal. One possible countermeasure is the creation of an approximate model that considers from the beginning the geometry stated in the supplier's combiners. One possible approach is represented in Figure 64. A displacement of 0.1mm (average PV value) was set in the middle of the part in the positive X-direction. Unfortunatelly, due to the lack of time it was not possible to run any simulations with this initial configuration.

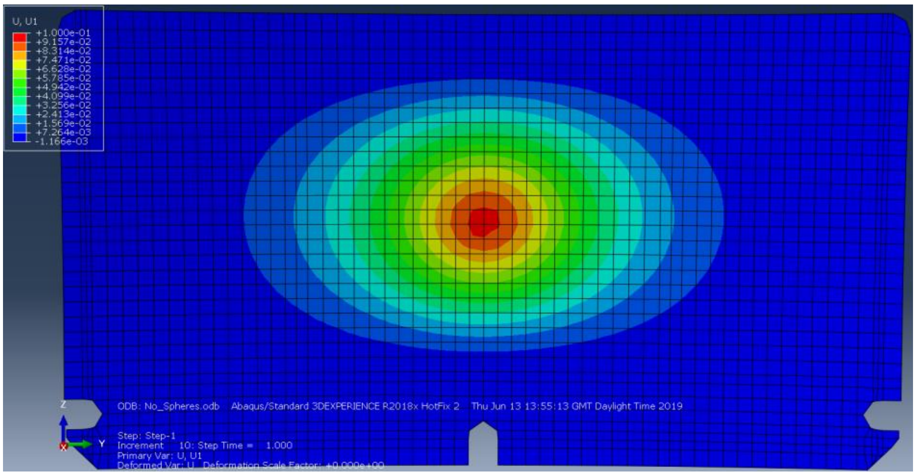

Figure 64: Approach to the nominal real part

The colors scale is not supposed to match perfectly the one used by the 3D scanner, although it is comprehensible that both results resemble the same deformation.

5.3 Combiners supports modifications and ABAQUS CAE simulation

In order to understand better the deformations the combiner was suffering, a batch of 5 combiner supports were measured and then modified.

To be able to identify the influence of the contact points, be it spheres or pads, in the geometry of the combiner after the gluing process, there were selected some combiner supports samples that were modified. As so, the selected combiner supports, numbered from 21 to 25, had either the spheres or the pads removed, in order to understand the magnitude of the deformation of each variable.

The specific modifications were the following:

Table 5 – Combiner support modifications

Combiner support and modification	Modification illustration
Combiner support 21 – All spheres removed	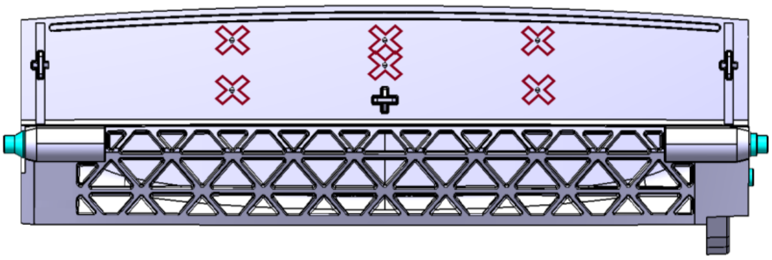
Combiner support 22 – All pads removed	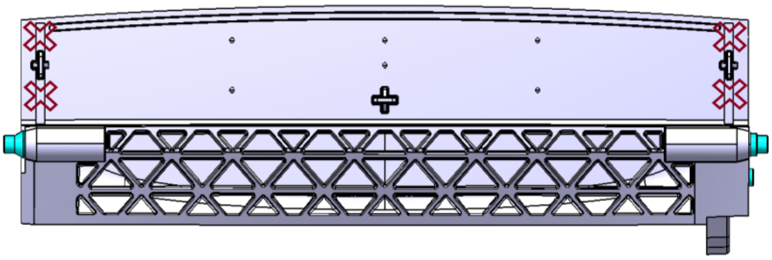
Combiner support 23 – Both side spheres removed	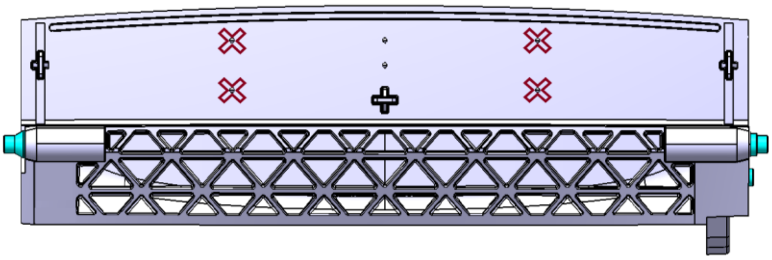
Combiner support 24 – Right side spheres removed	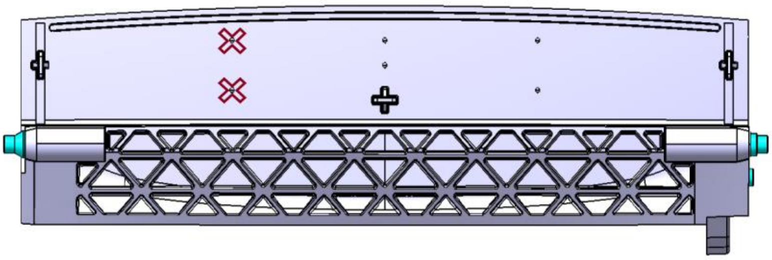
Combiner support 25 – Left side of the pads removed	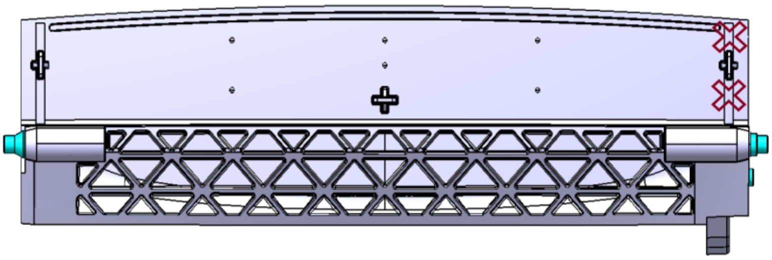

The combiner supports were measured previously to their modifications and after being altered. This way was possible to track down the obtained geometry after each modification. In doing so, it was possible to establish the inputs needed to test the created ABAQUS model.

The resultant combiner units fitted with the modified combiner supports were later studied in the 3D scanner in order to study what was the resulting deviation in the combiner. These results and the simulation model ones are going to be compared and analyzed further ahead in chapter 7. From Figure 65 to Figure 69 the ABAQUS simulation model output is represented.

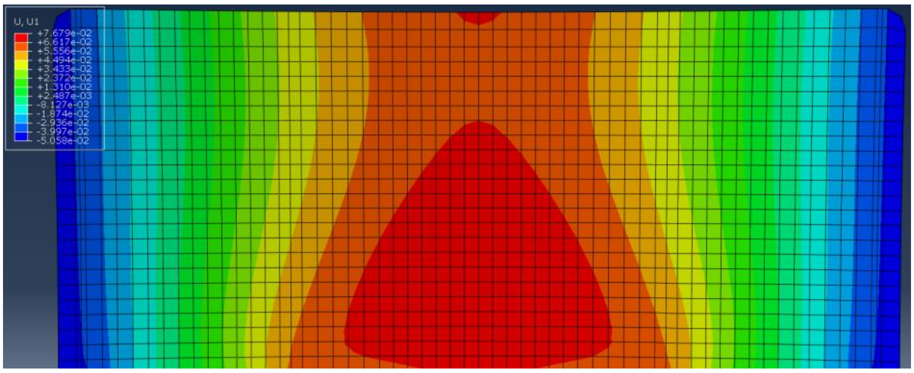

Figure 65: ABAQUS simulation of combiner unit 21

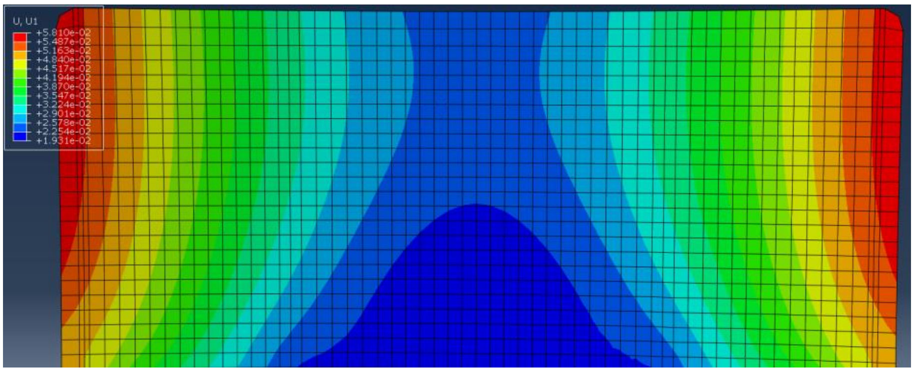

Figure 66: ABAQUS simulation of combiner unit 22

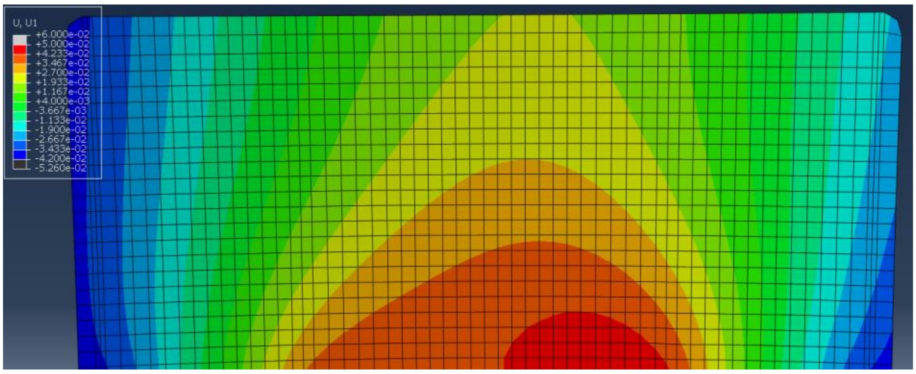

Figure 67: ABAQUS simulation of combiner unit 23

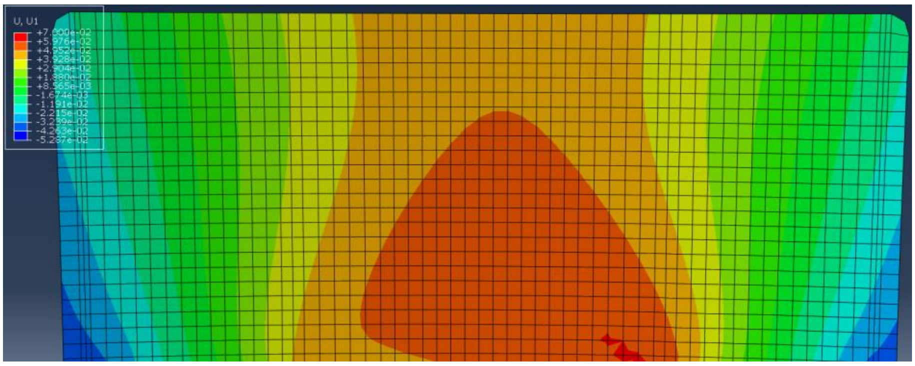

Figure 68: ABAQUS simulation of combiner unit 24

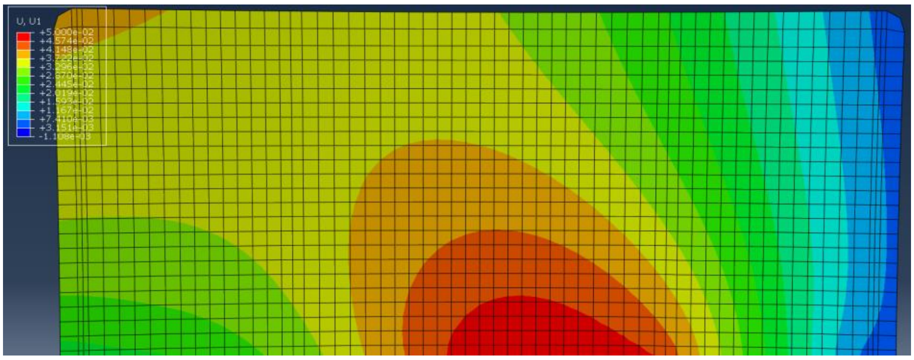

Figure 69: ABAQUS simulation of combiner unit 25

As referred before the analysis and comparison of the simulation results will be done ahead in chapter 7. Still, it’s important to state once again that the simulation model is being calculated considering the nominal CAD, and not counting with the initial deformations observed in the combiners before the gluing process, when it arrives from the supplier.

6 Jig development

In order to do experimental tests with the same controlled conditions as in the ABAQUS CAE simulation model, that is not considering the adhesive influence, a jig was developed using the CATIA V5 software (Figure 70). The jig was carefully designed to ensure that the optical geometry surface evaluation of the combiner wouldn’t be blocked by the jig surface and at the same time allow to study the effect the gluing process and the adhesive if they are not considered.

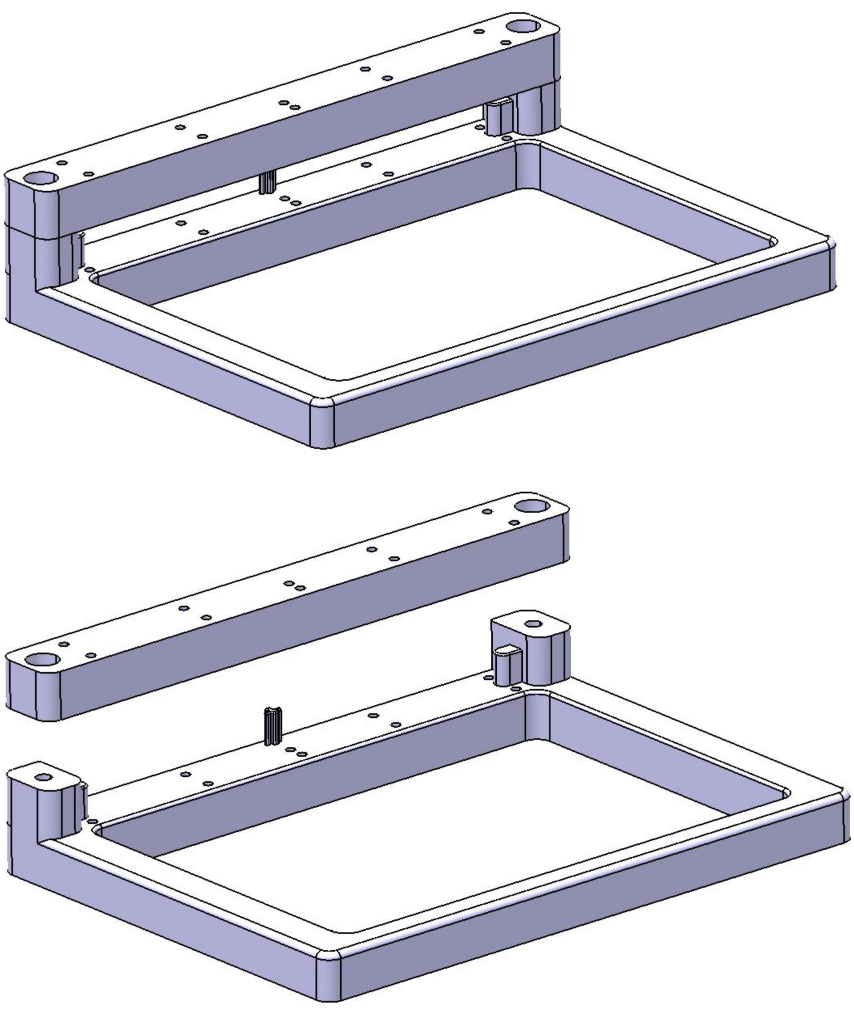

Figure 70: CATIA V5 model of the jig

The jig was printed using PLA (Polylatic Acid) as the building material. It is a biodegradable thermoplastic (under the correct conditions) and it’s derived from renewable resources such as sugarcane or corn starch. This material can be found in several applications ranging from plastic cups to medical implants. It is also one of the most popular bioplastics in the market. PLA also has a lower printing temperature when compared for example with the ABS, also very popular in 3D printing processes. This factor allows an easier printing since it's less likely for the material to warp when properly cooled and also allows the printing of sharper corners and features. (Giang, 2019) Some properties of PLA are stated in Table 6.

Table 6 – Polylatic Acid Properties (Giang, 2019)

Properties	PLA
Tensile Strength	37 MPa (0.2mm layer, 100% infill)
Elongation	6%
Flexural Modulus	4 GPa
Density	1.3 g/cm^3
Melting Point	173 ºC
Biodegradable	Yes
Glass Transition Temperature	60 ºC
Spool Price	22.99 USD
Common Products	Cups, Plastic Bags, Cutlery

6.1 3D printing simulation

Before printing the jig, a simulation was done to understand what would be the best parameters to select for the process.

Figure 71: Jig simulation

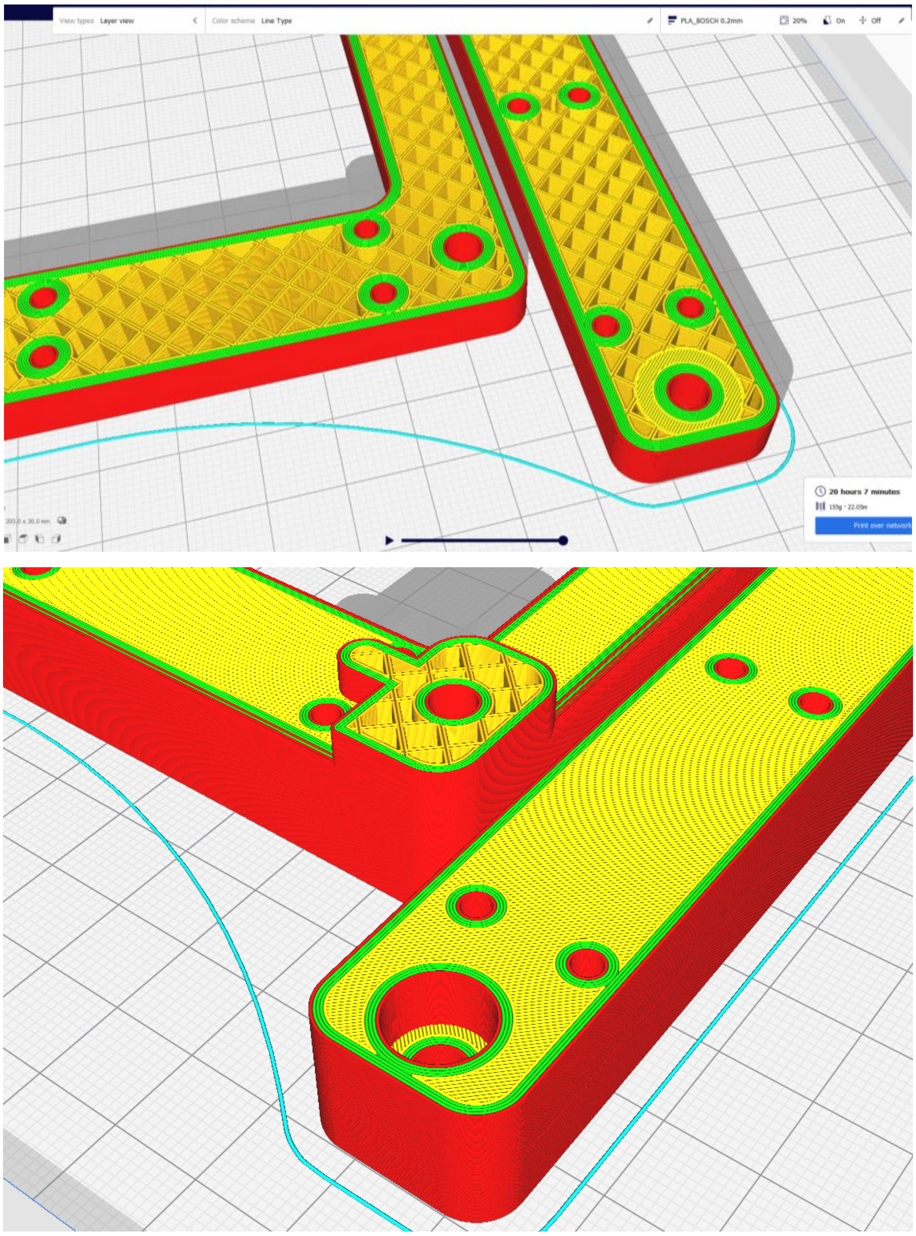

Figure 72: Jig feedrate simulation

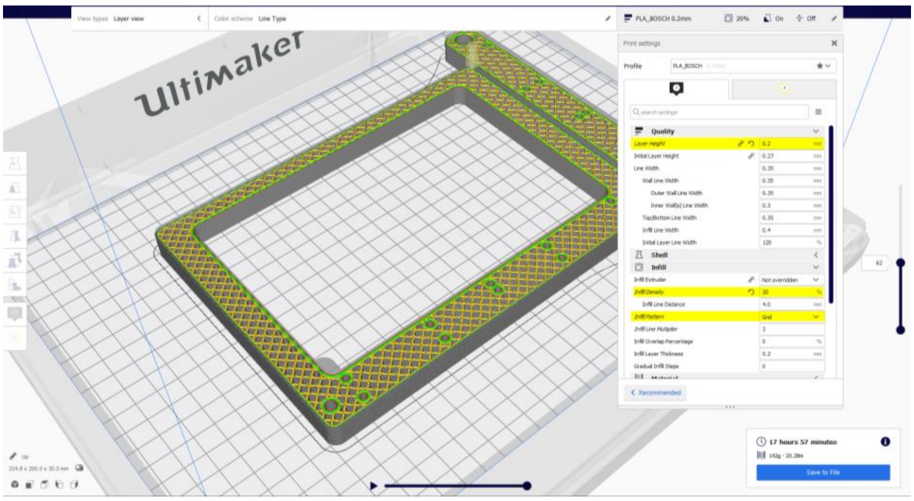

Figure 73: Selection of the printing parameters

According to the simulation, the production of the jig would take around 17 hours and 57 minutes. The parameters highlighted in yellow are the most important ones to define. Since the used printing method is technology that works layer by layer, the first highlighted parameters defines the layer height, that in this case was set as 0.2mm.

As for the second parameter, the infill density, the value set was 20%. This translates the amount of material used between the inner and the outer layer.

Lastly, the infill pattern chosen, as visible in Figure 73 was in a grid shape. This is a pattern that allows a good structural resistance.

These parameters, as well as the possible choices, are explained with more detail in chapter 7.2.

6.2 Jig production

After the model was created in CATIA V5 software it was produced in the Bosch prototyping lab. The jig was fully 3D printed. This allowed a quick production of the jig.

For the 3D printing a Ultimaker S5 3D printer was the printer used as shown in Figure 74.

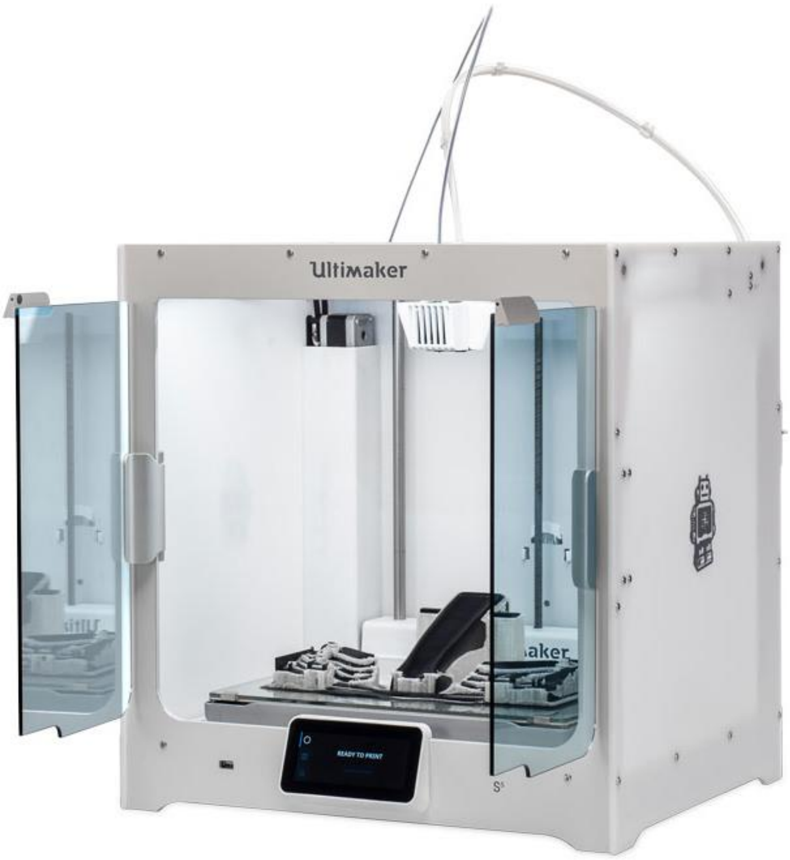

Figure 74: Ultimaker S5 3D printer

This 3D printer works with the FDM (Fused Deposition Modeling) principle, also called FFF (Fused Filament Fabrication). This is a printing technology, pioneered in the 1990s by Stratasys, that works both horizontally and vertically, having an extrusion nozzle moving over the building platform.

Followed by the upload of the digital design to the Ultimaker S5, the FDM printer starts printing. The raw material, in this case the PLA, is extruded as a thin filament, after having reached its melting point, through the heated nozzle. Once it is deposited at the bottom, the material solidifies. The part is then created layer by layer, knowing that each layer fuses with the layer below. In other words, the building of the object is from the bottom up. The process is explained in Figure 75.

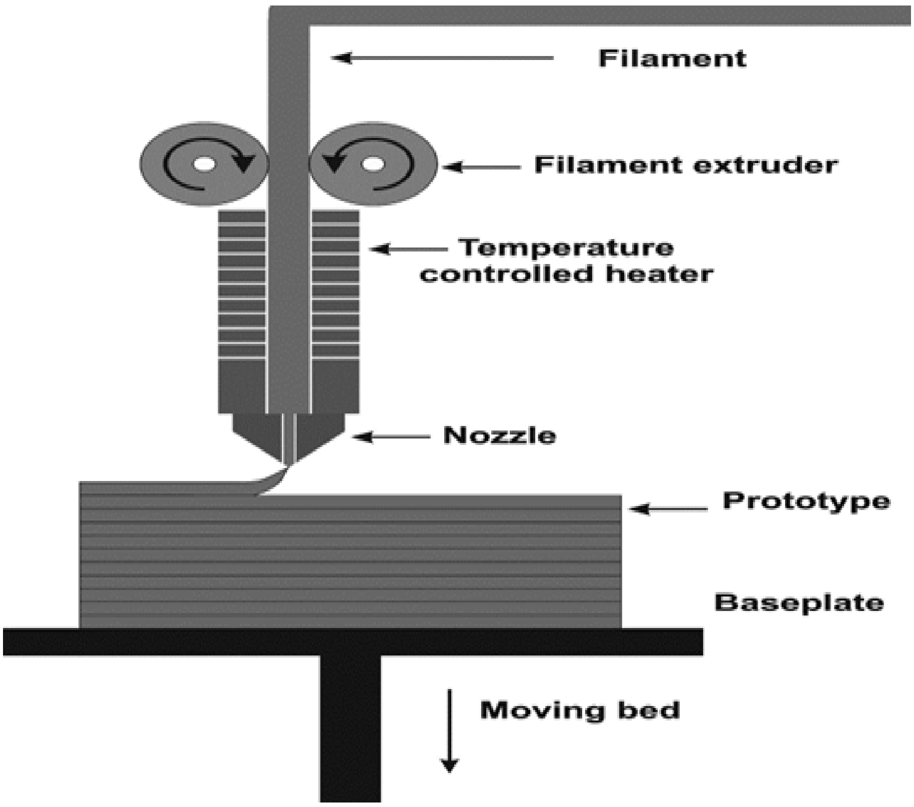

Figure 75: Schematic of a FDM printer (Olivera, 2019)

Generally, most FDM printers will first start by printing the outer edges, followed by the interior edges and lastly the interior of the layer which can be as either a solid layer or a fill in matrix. The infill process is one of the most important part of the process since it is responsible the resistance of the printed part and can be done in different shapes, sizes and even patterns as represented in Figure 76.

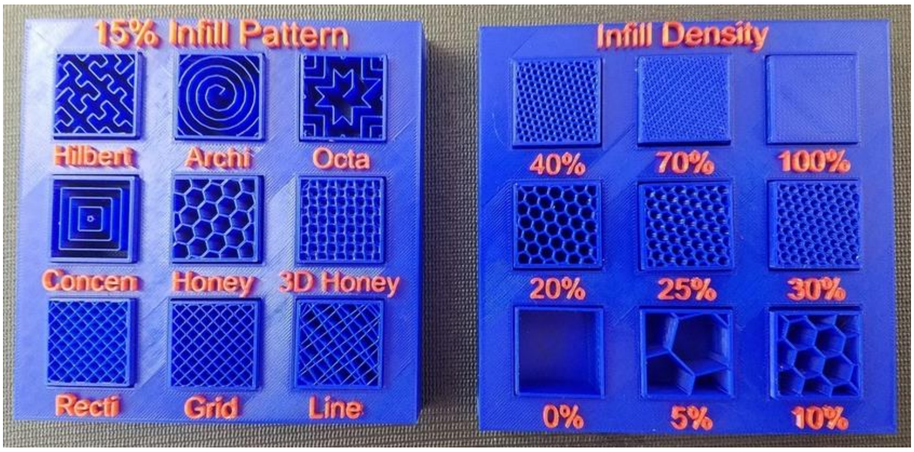

Figure 76: Infill pattern and density (Siber, 2019)

Once a style is defined it’s important to define the density for the infill. This choice depends on the desired strenght, structural resistance or even the mass. Starting with the mass, a higher infill density will lead to a heavier part. On the other hand, the less the density the more lightweight the part will be. Common infill densities are around 20% and 25%. Between these values we can have a great balance concerning durability and material consumption. If the cost is a concern and the structural part can be partially neglected, 10% to 15% of infill density is the best option. Otherwise, if a good structural part is requested the infill density should be between 30% and 50%. In case strength is the main request for a functional part, the percentage can be up to 100%. As referred before the jig was built with an infill density of 20% and for the infill pattern the shape selected was grid. As for the layer height the dimension set was 0.2mm. (Siber, 2019)

Using the FDM technology has several advantages such as being cost efficient, having less post-processing, providing flexibility in material choice and being easy handled. (Tractus3D, 2019) The main disadvantage is the lack of extremely high precision. Even tough, FDM printers have the precision recommended in this case to produce the desired jig. They are mainly used for creating prototypes for fit, form and function testing, creating and testing parts that can work under thermal loads, for rapid tooling patterns and mould inserts and, lastly, as stated before for the production of precise complex end-use parts as jigs and features. (DesignTech, 2019)

The jig is built of two parts, twenty-two bolts (twenty M3 and two M4) and two nuts. Two bolts and the two nuts only have an assembly function while the other twenty bolts are responsible for acting as the variables studied in the simulator, resulting in the deformation of the combiner.

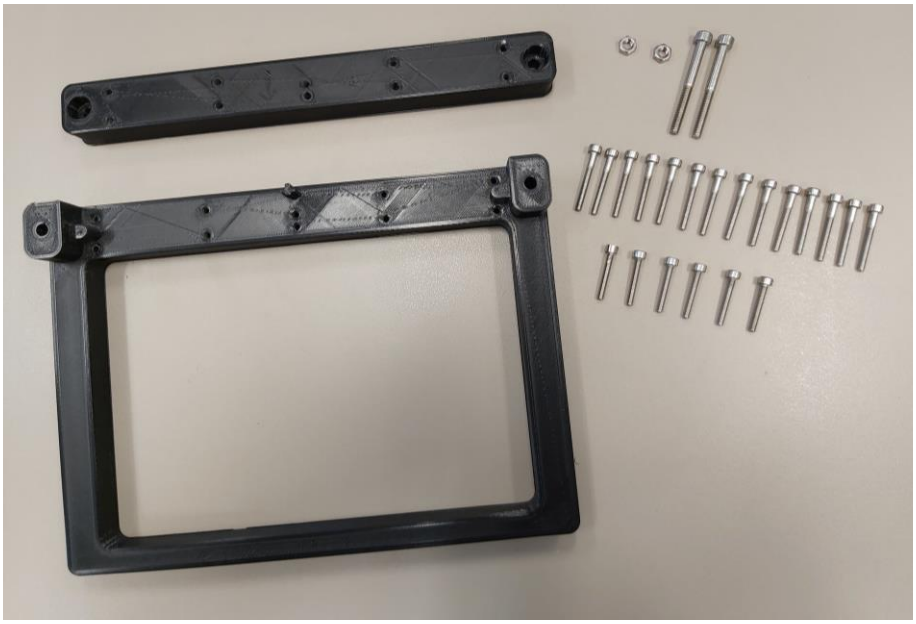

Figure 77: Jig components

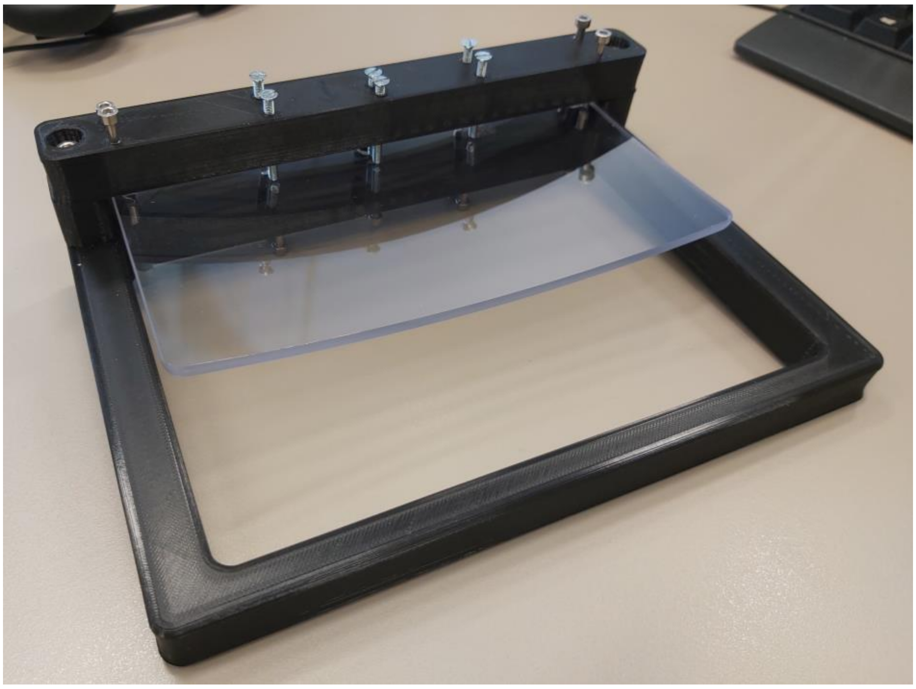

Figure 78: Final product

6.2.1 Base structure

Starting with the bottom part, also known as the base from now on, it's main function, apart from housing the bolts that will result in the deformation of the combiner, is to place the combiner in the correct position thanks to the guiding features built on it (Figure 79). A preliminar drawing was done where the two top supports of the base, located in top corners, were extended till the middle of the part. Ultimately, they were cut down to the size visible in Figure 79, ensuring the light would not be blocked by the jig surface and could then hit the full surface of the combiner. This will allow the correct measurement of the surface of the combiner by the 3D Shape scanner machine.

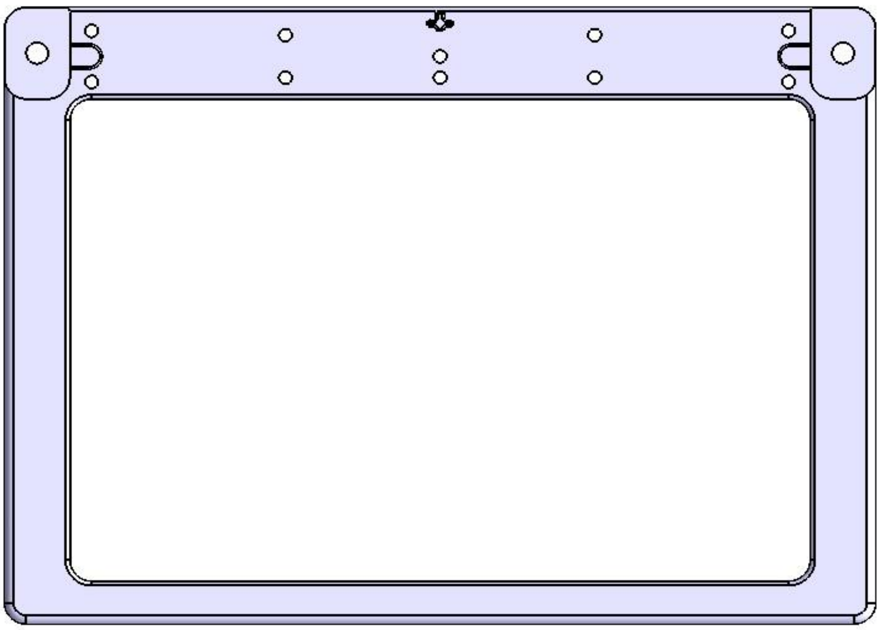

Figure 79: 3D Base model of the jig in CATIA V5

As referred before the bolts are placed in strategic points to simulate the P point's displacement. The displacement of the bolts can be adjusted by tightening or loosing them. Apart from supporting the combiner, the bolts can also be used for deformation as visible in Figure 80.

Figure 80: Jig base structure holding the combiner

6.2.2 Top part

Assembled to the base it's a top part in a rectangular shape in order to hold and allow the deformation of the combiner. It is assembled and tighten into the base structure with the help of two bolts M4 and it's fitted with ten bolts M3 that are loosened or tightened accordingly to the deformation that is desired to achieve. While the base pushes the combiner outer surface, the top part pushes the inner surface. This way it's possible to simulate the existence or not of the spheres and pads.

Figure 81: Top part of the jig

6.3 Working principle of the jig

The jig is a tool created to replicate the same conditions imposed in the ABAQUS CAE simulation model, and with that proceed to the simulation validation.

As referred before the combiner is mounted into the jig, to be then deformed taking into account the deviations of the combiner supports previously measured in the metrology lab at BOSCH. Taking into account the pitch of the used M3 bolts, the adjustment can be easily monitored.

In a first stage, the combiner supports selected are submitted to analysis in the metrology lab, allowing us to visualize how the component is deviated from the nominal measures. Then, the combiner selected to be mounted into the jig is fitted and the bolts are adjusted to a point where the combiner is just tighten, but not tensioned, avoiding the creation of tensions and deformation in an initial phase. It is important to have a combiner close to the nominal values, to increase the accuracy of the experimental testing. As visible in Figure 82, the combiner chosen and adjusted, has a low Peak-to-Valley, even when compared with the regular combiners used for this master thesis. This is important because the PV is the most global measured analyzed. Despite this fact, the combiner still is in a "BAD" condition due to the fact that the curvature parameters, responsible for detecting more local deviations, are out of tolerance.

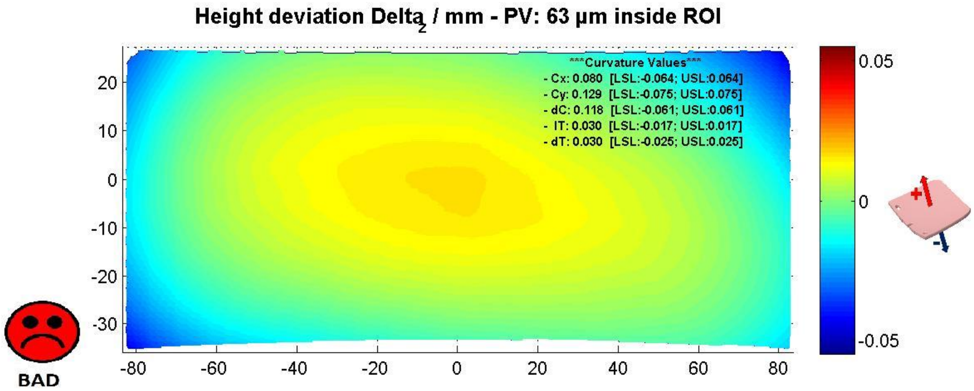

Figure 82: Initial phase of the combiner mounted in the jig

The combiner simply tighten is shown in Figure 83. The bolts are just touching the inner and outer surface of the combiner to avoid the combiner from moving. Besides the bolts, the jig has also three guiding features simulating the guiding features present on the combiner

Figure 83: Mounted and tightened combiner

Once the combiner is adjusted and confirmed there is no high PV or excessive torsion, the bolts can start to be tightened or loosened according to the measures obtained from the combiner supports measure in the metrology lab. Once adjusted to the correct positioning, the jig together with the combiner mounted in it, is analyzed in the 3D Shape scanner. This way we will be able to compare the results with the ones from the ABAQUS CAE simulation model, since conditions in both models are supposedly the same. In case the results match, we can proceed to the validation of the simulation model.

On the following chapter, the results of the analyzed combiners in the jig are shown and compare with the ABAQUS CAE simulation model for its simulation, as well as the combiners that had the combiner supports modified, in order to understand the impact of the entire gluing process, as well as the adhesive layer influence.

7 Validation of controlled model

In this chapter we will analyze the following results: the experimental tests on the jig, the combiner unit with the modified combiner supports and the ABAQUS CAE simulation. In order to validate the simulation and to have an understanding of the bonding process influence the three output results are compared.

Both output results of the combiner units with modified combiner supports and the combiners in the jig were taken with the 3D scanner machine, while the ABAQUS CAE simulation output was taken directly from the software. The results comparison will be done on chapter 7.1 and 7.2 based on a qualitative approach rather than quantitative.

7.1 Height deviation $Delta_z$ (PV Value) results comparison

One of the outputs of the 3D scanner is the color map in Height Deviation $Delta_z$ (PV value). This is one of the parameters chosen to be compared. It corresponds to the surface deviation analysis compared with the nominal measures. This will allow the comprehension of the shape of the combiner when mounted and if it's either getting more flat or if the curvature is more accentuated.

When comparing the ABAQUS CAE simulation model, it will be visible the color map will not follow the same exact color scale than the 3D scanner resulting images. It's then important to state that the color scale doesn't have the same resolution as the 3D scanner output results. Despite this fact, it will still be possible to do a plausible comparison between all results achieved.

The combiner units analyzed in the 3D scanner will be numbered from 21 to 25, following the same numbering done on the modified combiner supports on chapter 5.3. This will enable us to have a reference as to which modified combiner supports was mounted in each combiner unit.

An important note is the fact that the ABAQUS CAE simulation output might be slightly different due to the use of the nominal measures from the CAD part, instead of the measured real ones.

For the results comparison we will analyze each table separately.

In Table 7 we have the results from the combiner unit fitted with the combiner support 21 (all spheres removed). The analysis shows:

- Comparing the ABAQUS simulation model with the jig output it's visible that both results have the same color map distribution.
- Comparing the jig and the ABAQUS simulation model with the combiner unit measured in the 3D Shape scanner, the same color map distribution can be observed. It is even noticeable that all three output have the same tendency of getting narrower on top.
- As for the bottom of the combiner unit the ABAQUS and the 3D scanner are the more comparable due to larger width of the red are when comparing to the top. However, we can affirm that the combiner unit 21 simulation can be validated by the jig.

Table 7 - Combiner Unit 21 measuring results

Combiner Unit 21	**Height deviation Delta$_z$**
ABAQUS	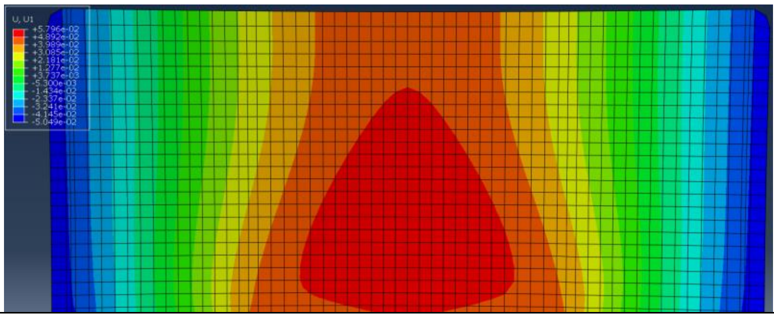
Jig	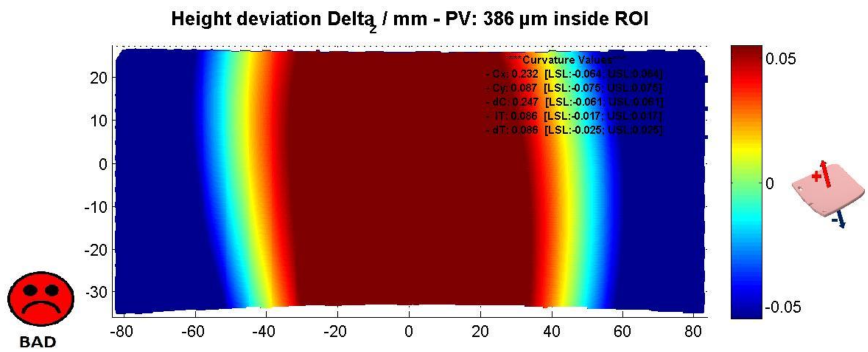
3D Scanner	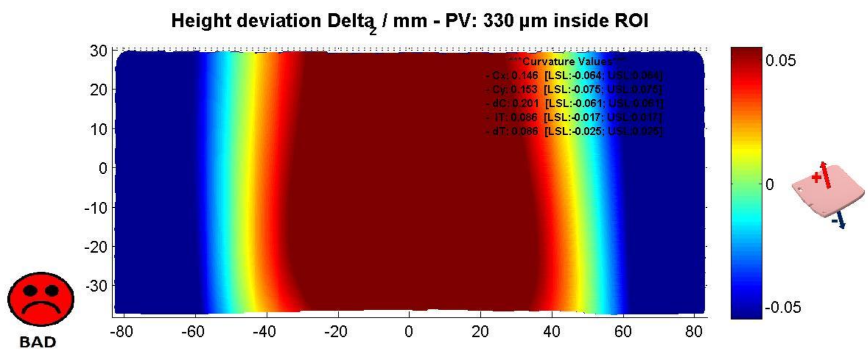

In Table 8 we have the results from the combiner unit fitted with the combiner support 22 (all pads removed). The analysis shows:

- The ABAQUS simulation model result and the result of the mounted combiner in the jig have a matching color map pattern. However, the jig has a more curved blue and red areas than the simulation output. This can be the result of the approximate material characterization of the combiner done on the ABAQUS simulation model.
- The jig and the 3D shape result, apart from the same color map distribution, it is also visible that the curvature lacking on the ABAQUS simulation model, exists in both cases. This can support the assumption made on the combiner material characterization. The 3D scanner is a bit twisted to the right, which can be due to the asymmetry of the combiner support used, which is a problem already discussed previously in this work.
- Apart from this small differences, the tendencies in all three results are similar which can lead us to the validation of the simulation, as well as the correct replication of the geometry by the jig.

Table 8 - Combiner Unit 22 measuring results

Combiner Unit 22	Height deviation $Delta_z$
ABAQUS	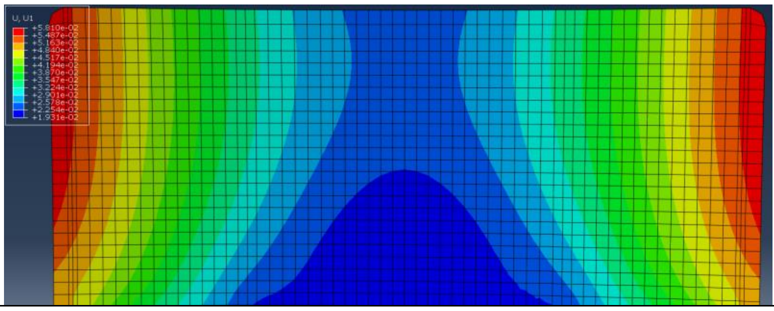
Jig	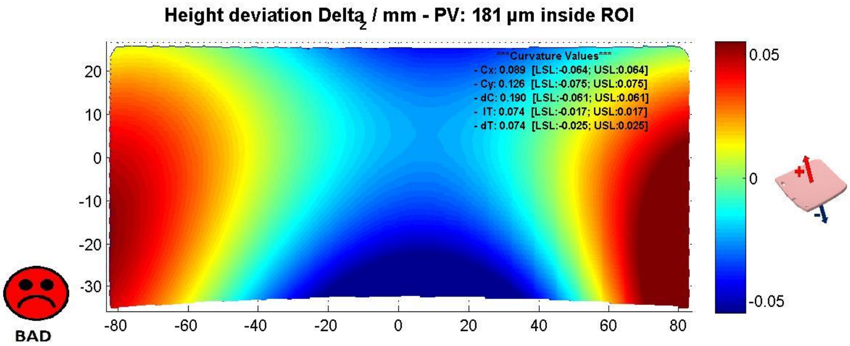
3D Scanner	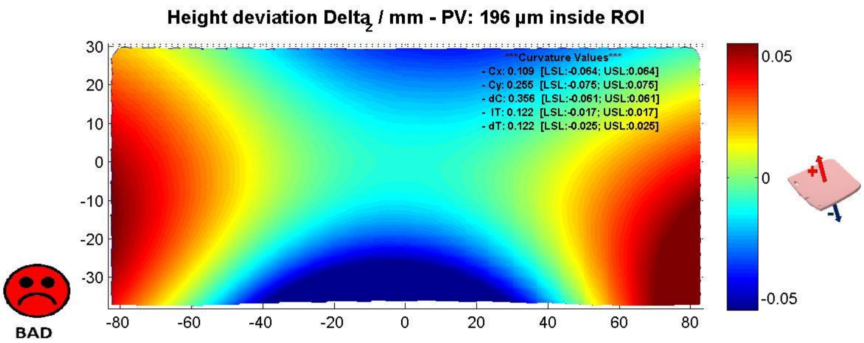

In Table 9 we have the results from the combiner unit fitted with the combiner support 23 (both side spheres removed). The analysis shows:

- A slight deviation to the right, even though both side spheres were taken out. Although it was expected for a symmetric color map, it was confirmed through the measurements done in the combiner supports that in the process of the removal of the spheres they were not equally removed. Besides this factor, the asymmetry of the combiner support due to the injection process can also be affecting the measures taken in the 3D scanner.
- Comparing the ABAQUS model with the jig model it is possible to see a higher influence on the right side in both cases. The same happens for the right bottom part of the red area. Still, in this case the ABAQUS model doesn't approach as much as in the other studied cases.
- In the jig we can see it is suffering from a bit of torsion. This might have happened due to an incorrect adjustment of the bolts in the pads area.
- Comparing the ABAQUS simulation model together with the 3D scanner it is possible to resemble one in the other, proving the validation of the simulation.

Table 9 - Combiner Unit 23 measuring results

Combiner Unit 23	**Height deviation Delta$_Z$**
ABAQUS	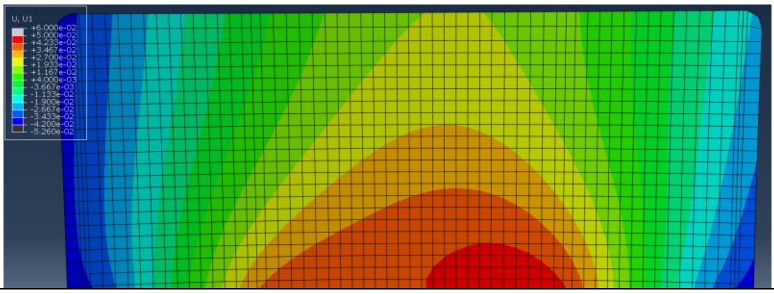
Jig	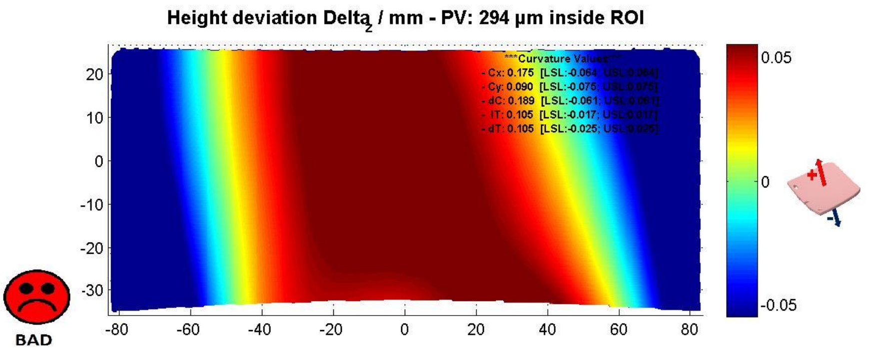
3D scanner	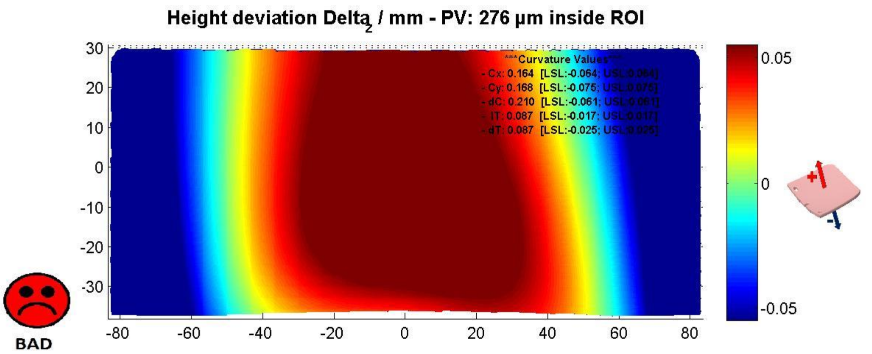

In Table 10 we have the results from the combiner unit fitted with the combiner support 24 (right side spheres removed). The analysis shows:

- Comparing both the ABAQUS simulation and the jig output, it's noticeable that they both have a correct deviation to the right in the red area caused by the elimination of the spheres on that side, and proved by the 3D scanner output.
- The bottom left part of red area despite not being equal on the three output, shows the same tendency as well.
- The ABAQUS simulation model and the 3D scanner output both have the exact same deviation on the left bottom of the red area.

Table 10 - Combiner Unit 24 measuring results

Combiner Unit 24	**Height deviation Delta$_Z$**
ABAQUS	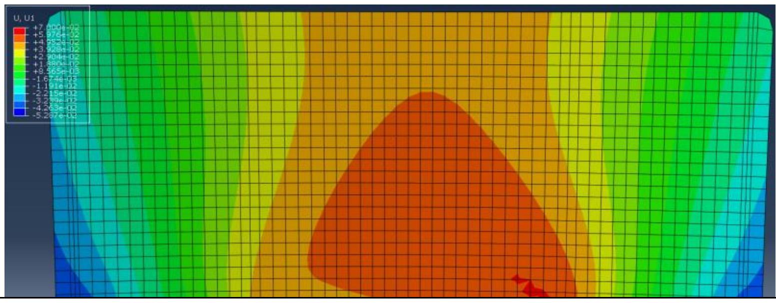
Jig	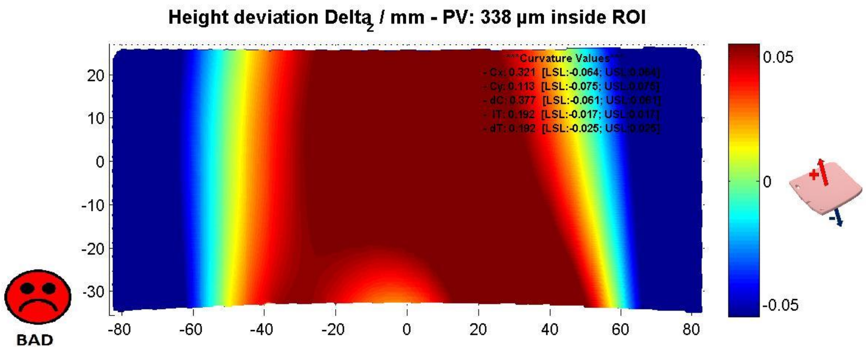
3D Scanner	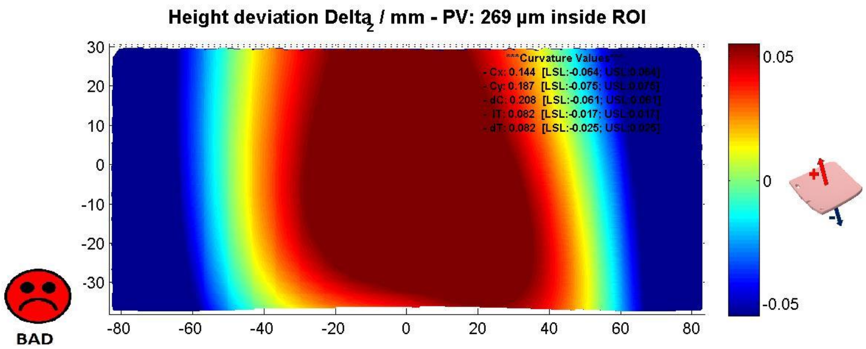

In Table 11 we have the results from the combiner unit fitted with the combiner support 25 (left side of the pads removed). The analysis shows:

- Comparing the ABAQUS and the jig results, there is a resemblance when it comes to the deviation suffered in the combiner, even though the jig deviation in the bottom starts more to the right than the simulation.
- Comparing the jig and the simulation model results together with the 3D Scanner output, there is a slightly decrease of the curvature in the last one. Apart from that, it´s visible that the red are is more saturated in both ABAQUS and jig results, telling us there is a higher influence in that particular zone than in the 3D Shape scanner sample.
- Although there is the existence of these small differences, the color map still looks very similar which provides us the validation of the simulation.

Table 11 - Combiner Unit 25 measured results

<table>
<tr><th>Combiner Unit 25</th><th>Height deviation Delta$_z$</th></tr>
<tr><td>ABAQUS</td><td>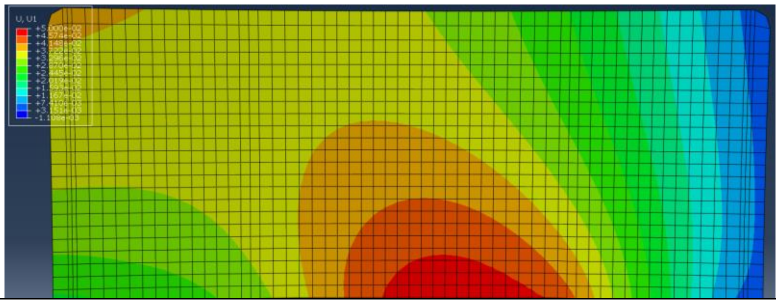</td></tr>
<tr><td>Jig</td><td>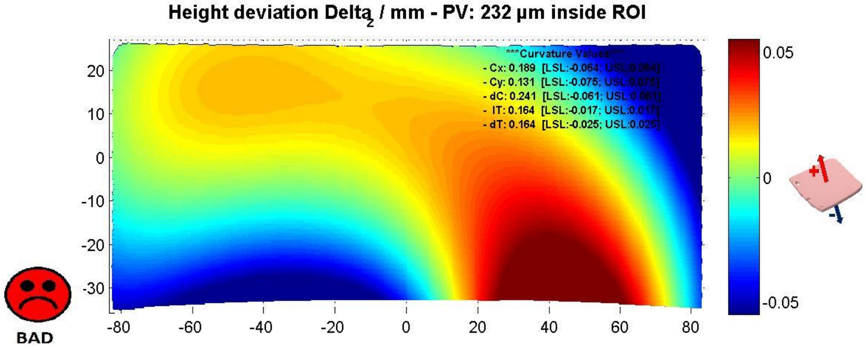
</td></tr>
<tr><td>3D Scanner</td><td>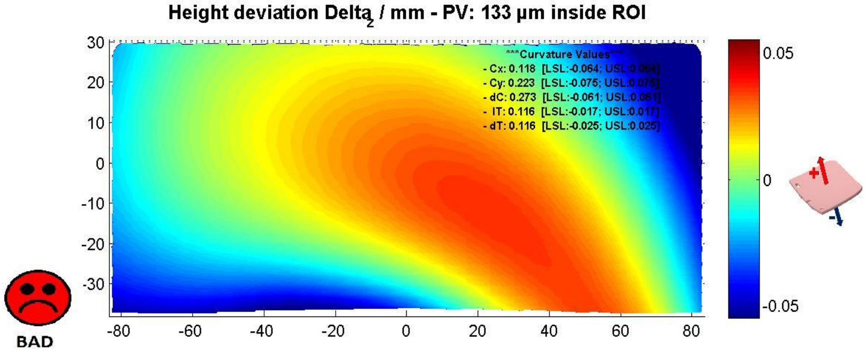
</td></tr>
</table>

7.2 Slopes results comparison

Till now it was possible to correlate both the 3D shape, the jig and the ABAQUS simulation model outputs, even though the last two don't take into account the influence of the entire gluing process as well as of the adhesive layer. Still, in this chapter the glue influence will be more visible and will allow us to understand the flaws of the ABAQUS simulation model and the jig when comparing with the real combiner unit measure in the 3D scanner.

Once again the combiner units analyzed are numbered from 21 to 25, corresponding to the fitted modified combiner support that had already been numbered from 21 to 25. Both the experimental jig results and the combiner units scanning results are related to different combiners, which can translate into different results, as the non-consideration of the adhesive influence. Nevertheless, we will analyze if the jig can replicate the same patterns as in the simulation so we can confirm the validation of it. Still, between these two sources and the real combiner units scanned in the 3D machine, there will always be some differences since we are starting off with different components. So, the results analysis will focus mainly on the color pattern tendencies.

Due to the amount of information it's difficult to have the figures in the tables with an appropriate size that can facilitate the reading of the user. But, since the analysis is based in a qualitative manner, in Table 12 is described how output results in the tables during this chapter are organized.

Table 12 – Diagram of the slope results tables

Combiner Unit ID	**Slopes measured in the 3D scanner output**
3D scanner output	Slope polynom in X direction ⇨ nominal ⇦ Slope polynom in Y direction A - Slope deviation in X direction B - Slope deviation in Y direction
Jig measurement output	Slope polynom in X direction ⇨ nominal ⇦ Slope polynom in Y direction A - Slope deviation in X direction B - Slope deviation in Y direction
ABAQUS simulation output	A - Slope deviation in X direction B - Slope deviation in Y direction

For the results comparison we will analyze each table separately.

In Table 13 we have the results from the combiner unit fitted with the combiner support 21 (all spheres removed). The analysis shows:

- The deformation in the center of the combiner in the X-direction in the jig is a bit deviated to the left side when compared to the ABAQUS simulation model and the 3D scanner output. This can be explained by the torsion of the combiner due to the adjustment of the bolts;
- A similar slope deviation in the X-direction between the 3D scanner output and the ABAQUS simulation model result;
- The slope deviation in the Y-direction in the ABAQUS simulation model is closer to the modified combiner unit than the jig, although the difference between the ABAQUS model and the jig is quite small. This can be explained by the influence of the adhesive and the gluing process, since this is not considered in both the jig and the simulation model.

Table 13 - Combiner Unit 21 measured slopes results comparison

Combiner Unit 21	Slopes	
3D Shape	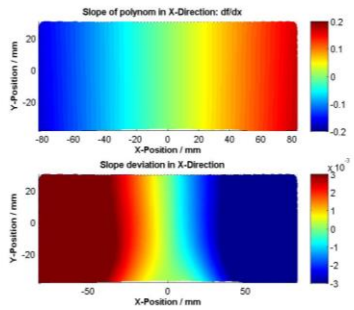 A	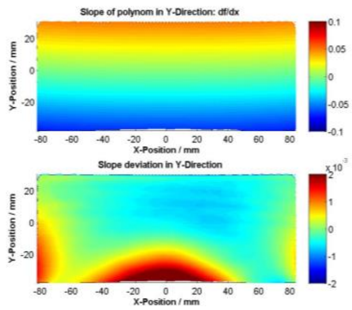 B
Jig	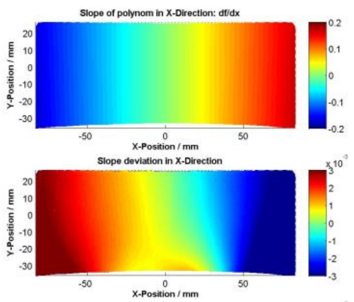 A	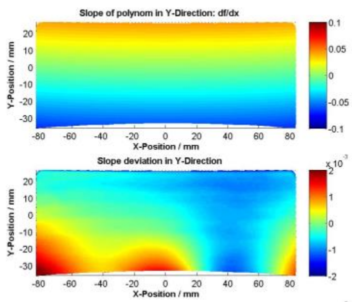 B
ABAQUS	A 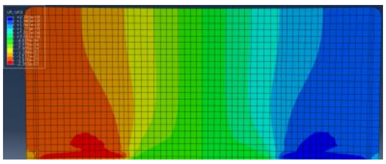	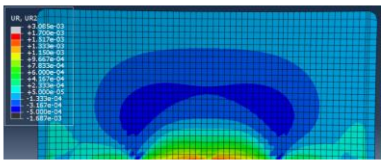 B

In Table 14 we have the results from the combiner unit fitted with the combiner support 22 (all pads removed). The analysis shows:

- Equal pattern in all the cases, with a bit more deformation in the jig than in the real mounted combiner. This is understandable by the fact that in the jig it's being applied a local displacement, rather than a distributed load like an adhesive layer.
- For the slope deviation in the Y-direction, the pattern also stays the same for the exception of the bottom center in the ABAQUS simulation model where there is a green area representing lower values when compared to the other two output results.

Table 14 - Combiner Unit 22 measured slopes results comparison

Combiner Unit 22	**Slopes**	
3D Shape	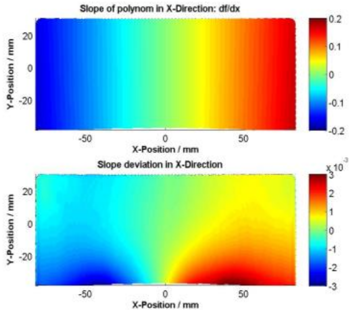 A	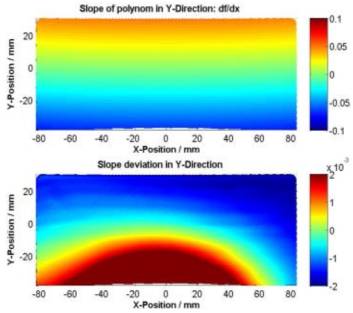 B
Jig	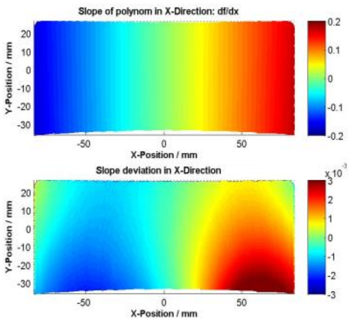 A	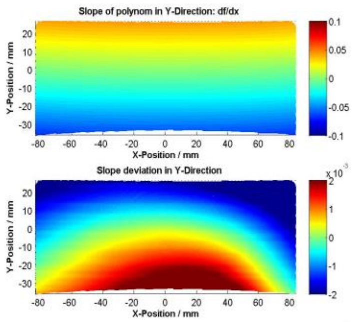 B
ABAQUS	A 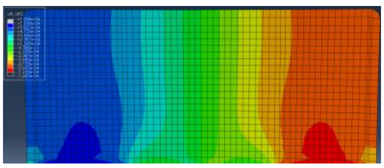	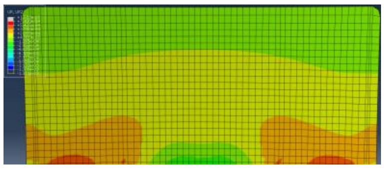 B

In Table 15 we have the results from the combiner unit fitted with the combiner support 23 (both side spheres removed). The analysis shows:

- In the X-direction both jig and ABAQUS simulation model have the same pattern as well as the bottom center detail, represented in red in the jig and in yellow in the simulation model.
- The pattern is the same for the 3D scanner output.
- The slope deviation in the Y-direction, the adhesive influence is clearly, creating a distributed deformation, while in both jig and ABAQUS outputs, instead of a distributed deformation, is a local deformation. Despite this, the results of the jig and ABAQUS allow us to validate the simulation model.

Table 15 - Combiner Unit 23 measured slopes results comparison

Combiner Unit 23	**Slopes**	
3D Shape	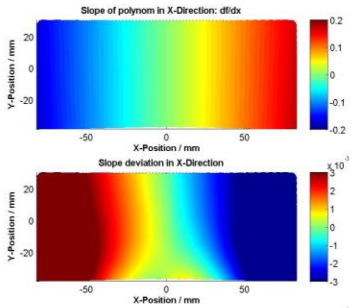 **A**	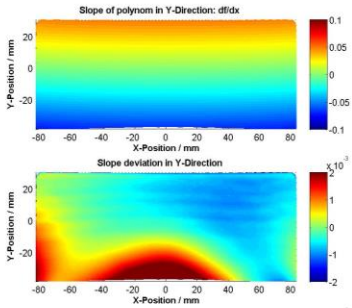 **B**
Jig	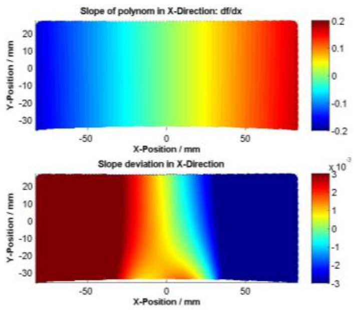 **A**	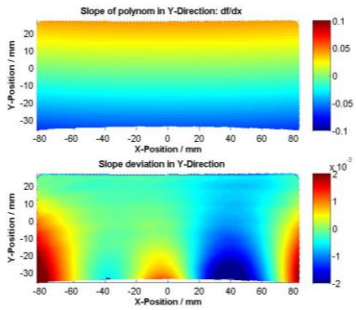 **B**
ABAQUS	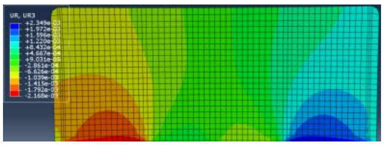 **A**	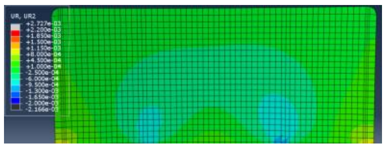 **B**

In Table 16 we have the results from the combiner unit fitted with the combiner support 24 (right side spheres removed). The analysis shows:

- In the slope deviation in the X-direction both jig and ABAQUS simulation model show the same pattern. It is possible to see in both outputs the same tendency in the bottom center, where the right side of the pattern has the tendency to be sharper in both figures.

- The slope deviation in the Y-direction the jig shows more local distributions, with a stronger effect on the right side and in the middle. Analyzing the ABAQUS result it is also visible a stronger distribution on the right side when compared to the left. As for the middle, represented in yellow in the jig, is visible the same distribution in the simulation model but, in this case in a green color.

- Comparing the jig and ABAQUS simulation model outputs with the modified combiner unit measured in the 3D scanner it is visible to see the same pattern in the X-direction.

- Comparing the jig and ABAQUS simulation model outputs with the modified combiner unit measured in the 3D scanner in the slope deviation in the Y-direction, there is almost no similarities. The most reasonable factor to consider here is the adhesive influence, since a pair of spheres was removed. So, instead of a local distribution the result is a more distributed displacement. Despite this, the simulation is validated by the jig output.

Table 16 - Combiner Unit 24 measured slopes results comparison

Combiner Unit 24	**Slopes**	
3D Shape	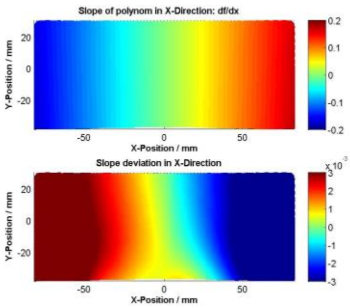 **A**	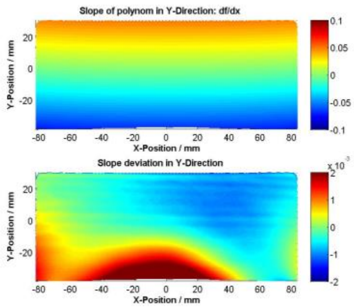 **B**
Jig	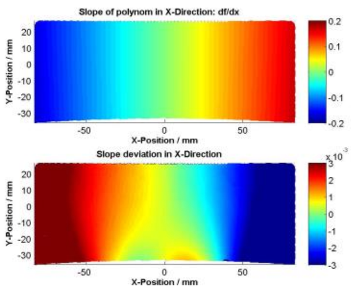 **A**	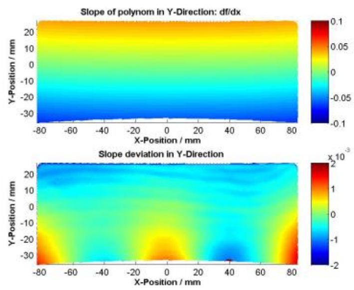 **B**
ABAQUS	**A** 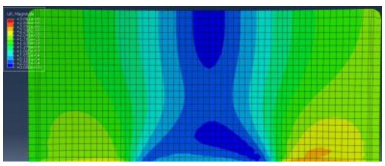	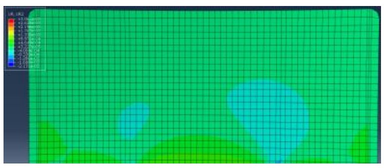 **B**

In Table 17 we have the results from the combiner unit fitted with the combiner support 23 (left side of the pads removed). The analysis shows:

- The jig and ABAQUS results have some similarities and some factors that don't correspond. For the analysis of the slope deviation in the X-direction, both outputs have the same round distribution in the bottom part. Still, comparing the left side of the combiner, although there is the blue region in the same spot in both, the red region that appears in the jig output is not visible in the simulation model output. This can be due to the fact of being needed a more precise material characterization of the combiner in the simulation model.
- Comparing the jig with the 3D scanner the red zone matches, even if in different scales.
- Comparing the three outputs from the slope deviation in the Y-direction, the same pattern is visible in all cases, despite one being more rounded than other. Having analyzed both variables, we can once again state that the simulation can be validated.

Table 17 - Combiner Unit 25 measured slopes results comparison

Combiner Unit 25	**Slopes**	
3D Shape	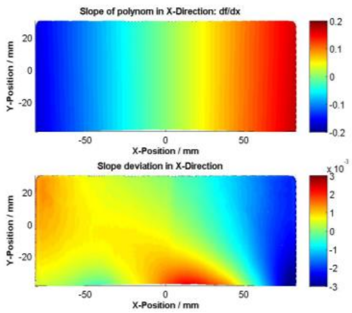 **A**	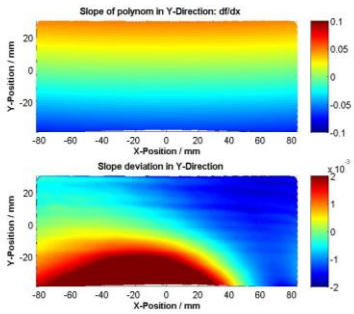 **B**
Jig	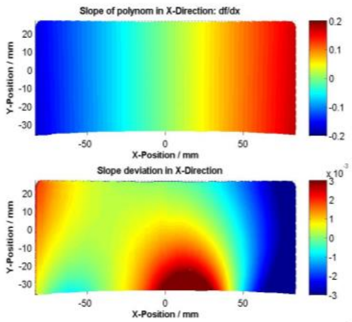 **A**	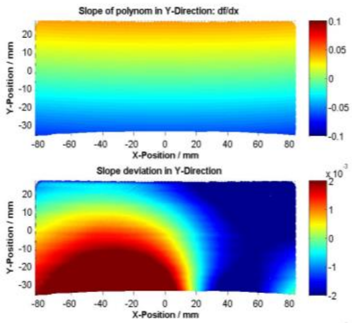 **B**
ABAQUS	**A** 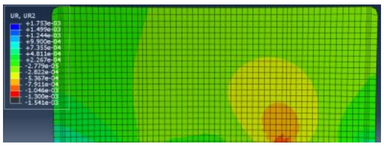	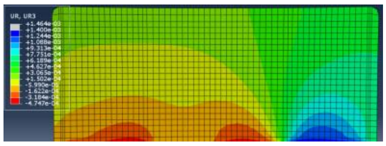 **B**

In a general review, for the height deviation (PV value), which is the deviation of the surface compared to the nominal measures, all results are very similar when comparing the three different sources, the 3D Shape, the jig and the simulation model.

On the other hand, the slope results might show a small difference since the adhesive is not being considered in both the jig and the simulation model as referred previously.

8 Conclusions and Future work

8.1 Final conclusions

As proposed at beginning of this thesis, the main goal was to understand how the combiner geometry changes, taking into account the shape deviation from the combiner support, as well as the influence the gluing process has on the deformation of the combiner units.

The first conclusive analysis is the fact that the gluing process does imposes deformation in the combiner geometry. For this study, a batch of parts was measured previously and after the gluing process. The analyzed data consisted of the PV value and the curvature parameters. While the PV value could increase or decrease depending on the combiners, the curvature values of all the combiners had their values risen up to the double. On a more qualitative approach, it's clearly visible through the 3D shape scanner output data that the initial deformation of the combiner that had a circular shape, turns into a different shape that confirms the existence of deformation.

An ABAQUS CAE simulation model was created to allow us to forecast what impact the deformed combiner supports would have on the combiner geometry after the assembling process. The combiner geometry study on this simulation was done based on the influence of the contact points of the combiner support, but not considering the effect of the adhesive layer, responsible for the bonding of both parts.

With the forecasts done for the extreme shape deviations considered on the contact points of the combiner and combiner support, a batch of five combiner supports was submitted to the metrology lab for being measured. All samples were later modified in order to meet the imposed conditions of the simulation model. These modifications consisted on the removal of several different points of contact, depending from each combiner support. Followed by the modifications, the five samples were once again measured in the metrology lab and afterwards taken to the production line in order to be assembled together with combiners that were also previously analyzed. The output data obtained from the resulting combiner units matched the one obtained from the simulation model, only lacking some precision in the cases where the influence of the distributed load created by adhesive layer was important to consider.

To fully understand the importance of the shape deviations of the combiner supports an experimental model was created. This model replicated the same conditions imposed on the simulation, meaning that it can allow the variation of all the contact points. The combiner would be later scanned in the 3D Shape machine and the results compared with the modified parts and the simulation model. This confirmed the veracity of the output of the experimental model as well as a validation of the simulation model, demonstrating that the simulation could be a valid model to forecast the combiner geometry in a qualitative way.

In summary, both the deviations of combiner supports, as well as the gluing process and the adhesive layer have influence on the combiner unit geometry. Still, it was observed that the pads deviations had a greater influence when compared to the spheres deviations. The simulation can reproduce the geometry while the jig can replicate the imposed conditions in the ABAQUS model and validate it.

8.2 Future work

In order to increase the precision of the simulation the polycarbonate material that composes the combiner should be characterized.

The simulation can be performed by introducing the adhesive layer and its influence on the combiner, as well as a full simulation of the entire assembly of the combiner unit. An initial state of the combiner considering the initial deformation was studied during this work. Although, due to the lack of time it was not possible to implement it in the simulation.

Also due to the lack of time, a final propose for a future work is the implementation of a code that can take the ABAQUS simulation model, create an output matrix and then submit it to the optical software used by the optical department.

9 Bibliography

Ajri, A. (2016, May 26). *3DS Academy*. Retrieved May 2, 2019, from https://academy.3ds.com/en/projects/finite-element-modeling-using-abaqus

Almeida, R. (2019). *Head-up Display Combiner Unit stress and deformation analysis.* Retrieved March 05, 2019

Andujar Moreno , R. (2011, July 17). *Stochastic and Lagrangian*. Retrieved May 2, 2019, from http://stochasticandlagrangian.blogspot.com/2011/07/what-does-shape-function-mean-in-finite.html

B. Mouhmida, A. I. (2006). *A study of the mechanical behaviour of a glass fibre reinforcedpolyamide 6,6: Experimental investigation.* Retrieved May 03, 2019

Bosch. (2019, January 4). *Bosch*. Retrieved June 6, 2019, from https://www.bosch.com/our-company/our-figures/

Bosch, R. (2019). *Bosch em Portugal*. Retrieved from https://www.bosch.pt/a-nossa-empresa/bosch-em-portugal/

Bosch, R. (2019). *Bosch Figures*. Retrieved from https://www.bosch.com/our-company/our-figures/

Broekaart, D. (2015). *Dutch High Tech*. Retrieved May 21, 2019, from https://www.dutchhts.nl/company/simuleon/

DesignTech. (2015). *DesignTech*. Retrieved JuNE 06, 2019, from https://www.designtechsys.com/articles/working-fdm-3d-printers

Evans, M. (2013, June). *Shout! Outdoor Lifestyle Magazine*. Retrieved May 2, 2019, from http://www.shoutlifestyle.com/lead-dog-fac

FORD. (2018, June 21). *FORD Media Center*. Retrieved May 2, 2019, from http://www.campaign.ford.com/campaignlibs/content/fordmedia/feu/fr/fr.relatedmedia.viewmore.image.html/content/fordmedia/feu/fr/fr/news/2018/06/21/la-nouvelle-ford-focus-s-inspire-des-avions-de-chasse-pour-garde/jcr:content/rightRailPar/relatedmedia.html

Giang, K. (2019). *3DHubs*. Retrieved June 06, 2019, from https://www.3dhubs.com/knowledge-base/pla-vs-abs-whats-difference

GRAITEC. (2019). *GRAITEC GROUP 2019*. Retrieved May 21, 2019, from https://www.graitec.com/finite-element-analysis-fea/

Kuusisto, E. (2017). *SHELLS vs. SOLIDS | Finite Element Analysis Quick Review*. Retrieved May 17, 2019

McKeen, L. W. (2014). *The Effect of Temperature and other Factors on Plastics and Elastomers (Third Edition).* William Andrew Publishing. Retrieved June 7, 2019, from Science Direct.

McNamara, P. (2018, July 03). *Car Magazine*. Retrieved May 02, 2019, from https://www.carmagazine.co.uk/car-news/first-official-pictures/ford/new-ford-focus-2019-uk-price-interior-pictures-specs-engines-and-release-date/

Mecum, D. (2016, November 05). *Mecum Auctions*. Retrieved May 02, 2019, from https://www.mecum.com/lots/DA1116-272552/1930-ford-model-a-town-sedan/

Neiger, C. (2012, April 17). *HowStuffWorks*. Retrieved June 2019, 13, from (https://auto.howstuffworks.com/car-driving-safety/safety-regulatory-devices/head-up-display1.htm)

Nicolazzo, J. (2013, Junho 15). *Auto Spies*. Retrieved May 02, 2019, from http://www.autospies.com/news/BMW-4-Series-Offers-The-Newest-Full-Color-Heads-Up-Display-For-The-New-Model-76642/

Olivera, S. (2016, January). *ResearchGate*. Retrieved June 06, 2019, from https://www.researchgate.net/figure/Schematic-of-an-FDM-3D-printer-Reproduced-with-permission-from-12_fig1_292985550

Roze, G. (2018, July 20). *StockCharts*. Retrieved May 03, 2019, from https://stockcharts.com/articles/journal/2018/07/your-dashboard-to-navigating-the-markets---chartpack-update-20-q2-2018.html

Siber, B. (2019). *All3DP*. Retrieved June 06, 2019, from https://all3dp.com/2/infill-3d-printing-what-it-means-and-how-to-use-it/

Silva, L. F. (2007). *Juntas adesivas estruturais.* Publindústria.

Smith, A. (2014, December 09). *AutoCar*. Retrieved May 02, 2019, from https://www.autocar.co.uk/car-news/motoring/history-peugeot-205-gti-%E2%80%93-picture-special

ThreeBond. (2019). *ThreeBond*. Retrieved May 02, 2019, from https://www.threebond.co.jp/en/technical/seminar/epoxy.html

Tractus3D. (2019). *Tractus3D*. Retrieved June 06, 2019, from https://tractus3d.com/what-is-3d-printing/fdm-3d-printing/

York, C. f.-U. (2013, March 18). *The Essencial Chemical Industry - Materials and Applications*. Retrieved May 24, 2019, from http://www.essentialchemicalindustry.org/materials-and-applications/composites.html#aramid

York, C. f.-U. (2016). *The Essential Chemical Industry - Polymers*. Retrieved May 24, 2019, from http://www.essentialchemicalindustry.org/polymers/polyamides.html

Appendix A: Other activities

During the internship at BOSCH Car Multimedia in Braga, besides the master thesis other activities related to the CM-CI2/ECM3 were realized.

1. **Use of the Kanban and Scrum methodology**

   The team uses the Kanban board methodology in order to organize all the activities that have to be performed during the elapsed time of four weeks. There were three meetings per week, to analyze the ongoing tasks and, at the end of the month a longer meeting was done to plan the following four weeks. This was very beneficial in the organization of the tasks for my master thesis.

2. **Visit to BMW production line**

   Apart from the time I spent in the FORD production for the understanding of the entire process, it was also done a visit to the BMW production line, to observe the differences in the processes for the production of the two similar components.

3. **Adhesive thickness measurement presentation**

   Following the adhesive thickness measurements done on this master thesis a presentation was prepared with all the valuable data that could be useful for the team to use in the understanding of the components problems.

4. **Combiner surface roughness measurement**

   Asked by BOSCH, a sample of combiners that had a sand blasting treatment were measured using a Hommelwerke LV-50. This machine uses a diamond tip with 5 µm radius and has a range amplitude of -300µm to 300µm.

5. **Shims experimental testings**

   In another attempt to understand the influence of the combiner support deviations in the combiner geometry, some shims were used to lift some control points and the the parts were submitted to the gluing process and later measured in the 3D scanner machine.